Spring 5-31-1993

Tantalum silicide variable capacitance rotary micromotors : design and fabrication

Michael Steven Berry
New Jersey Institute of Technology

ABSTRACT

Tantalum Silicide Variable Capacitance Rotary Micromotors - Design and Fabrication

by
Michael Steven Berry

Tantalum silicide was studied as an alternative microelectromechanical material by fabricating a rotary micromotor utilizing a proven design. This material was used for the rotor, stators, and bearing over a silicon substrate. It has the attraction of potentially reducing the friction which is a major problem with polysilicon-to-polysilicon bearings.

The necessity of high aspect ratio features required that a plasma or reactive ion etch with a high degree of anisotropy be developed to etch tantalum silicide films in excess of 1.5μm. A sulfur hexafluoride/Freon 115 plasma provided the necessary process control during the etches. The stress present in annealed tantalum silicide films made it necessary to limit the maximum processing temperature to 300°C. These low temperature tantalum silicide films have thus far proved to be inadequate as a microelectromechanical material for the micromotor due to their inability to withstand the hydrofluoric acid release etch.

TANTALUM SILICIDE VARIABLE CAPACITANCE ROTARY MICROMOTORS - DESIGN AND FABRICATION

by
Michael Steven Berry

A Thesis
Submitted to the Faculty of
New Jersey Institute of Technology
in Partial Fulfillment of the Requirements for the Degree of
Master of Science in Electrical Engineering

Department of Electrical and Computer Engineering

May 1993

APPROVAL PAGE

Tantalum Silicide Variable Capacitance Rotary Micromotors - Design and Fabrication

Michael Steven Berry

Dr. William N. Carr, Thesis Advisor (date)
Professor and Holder of Sponsored Chair in Microelectronics, NJIT

Dr. Durgamadhab Misra, Committee Member (date)
Assistant Professor of Electrical Engineering, NJIT

Dr. Nuggehalli M. Ravindra, Committee Member (date)
Associate Professor of Physics, NJIT

Michael J. Grieco, Committee Member (date)
Assistant Research Professor of Microelectronics, NJIT

BIOGRAPHICAL SKETCH

Author: Michael Steven Berry

Degree: Master of Science in Electrical Engineering

Date: May 1993

Undergraduate and Graduate Education:

- Master of Science in Electrical Engineering,
  New Jersey Institute of Technology, Newark, NJ, 1993

- Bachelor of Arts in Physics,
  Drew University, Madison, NJ, 1989

Major: Electrical Engineering

Presentations and Publications:

Berry, Michael S., and Supplee, James. "Rocket on a Spring." *European Journal of Physics*, Volume 11, Number 3, 1990.

To Kelly

ACKNOWLEDGMENT

The author wishes to express his sincere gratitude to his thesis advisor, Dr. William N. Carr, for his continued support throughout this research.

Special thanks to Professors Durgamadhab Misra, Nuggehalli Ravindra, and Michael Grieco for serving as members of the committee.

The author is grateful to the State of New Jersey for initial funding of the research, through the Sponsored Chair in Microelectronics, and to the Microelectronics Research Center for its continued funding and assistance.

The author thanks Dr. Robert J. Zeto and Charles Mulford of the U.S. Army Research Laboratory in Ft. Monmouth, NJ, for their guidance and cooperation during the initial phase of the research.

The author thanks Stephen Bart for his helpful discussions during the design phases of the micromotors. They helped avoid many problems in the mask set. Thanks also to Professor Dan Cho at Princeton University for making those meetings possible.

The author is especially grateful to Michael Grieco, Lab Manager of the Microelectronics Research Center at NJIT, for his invaluable guidance and foresight throughout this project. Without his cooperation, this research could never have been completed.

TABLE OF CONTENTS

Chapter **Page**

LIST OF TABLES

LIST OF FIGURES

Figure **Page**

CHAPTER 1

INTRODUCTION

1.1 Thesis Description

This thesis presents processing techniques and results from the design and fabrication of side drive variable capacitance rotary micromotors (hereafter referred to as micromotors) using tantalum silicide ($TaSi_2$) as the primary microelectromechanical material. The primary objective of this work was to utilize existing models for micromotor design and to introduce $TaSi_2$ for the first time as a micromotor material for the rotor and stators. Tantalum silicide was expected to reduce friction in the devices and therefore to increase motor lifetime as compared to a similar device fabricated with LPCVD (low pressure chemical vapor deposition) polysilicon.

Tantalum silicide was chosen for several reasons. It is a low resistivity material compared with polysilicon (approximately an order of magnitude lower); it is capable of withstanding high temperatures (900°C) without significant grain growth; it is compatible with standard VLSI processing techniques; and most importantly, the surface roughness of tantalum silicide as compared with a typical polysilicon film is much less (the grainsize is too small to be seen at 1000X). In addition, the microhardness of $TaSi_2$ is significantly higher than that for many other silicides, and it should therefore be well suited as a bearing material. The microhardness of $TaSi_2$ and other silicides is given in Table 1.1.

Chapter 1 presents a brief history of micromachining and micromotors, including both surface micromachined devices and motors fabricated by the LIGA process. Chapter 2 reviews the principle of operation of the micromotor, including a derivation of the torque equations for the motors and the requirements for the drive circuit for the motors

being considered here. The micromotor design is discussed in Chapter 3. The discussion includes motor geometry considerations, justification for the use of LOCOS, and dimensional considerations used in the mask layouts. The core of the thesis lies in Chapters 4 and 5, where the device fabrication is discussed. Chapter 4 concentrates on the general fabrication sequence that was followed, and includes some of the problems unique to using tantalum silicide. Chapter 5 focuses on the etch characteristics of thick tantalum silicide films, including a discussion of both wet and dry etches. A novel application for rotary micromotors, or a functional variation thereof, is presented in Chapter 6. A summary and conclusions as to the practicality of using $TaSi_2$ as a micro-electromechanical material for future devices are given in Chapter 7. Also discussed are suggestions for future work with $TaSi_2$.

Table 1.1 Microhardness of some silicides [23]

Silicide	Microhardness, 100g load (kg/mm^2)
$TaSi_2$	1407
$TiSi_2$	892
WSi_2	1074
$CoSi_2$	77-552

1.2 Background

Operational variable capacitance rotary micromotors fabricated with silicon micromachining techniques have been in existence for several years [1-4]. The principle material used for their fabrication has been polysilicon, largely because of its compatibility

with standard IC processing, its ability to be doped to be a conductor, its ability to withstand hydrofluoric acid (HF) for the release process, and its mechanical stability.

One of polysilicon's major negative properties however is the roughness of its surface. This roughness is due largely to grain growth during the high temperature doping of the polysilicon, and is difficult to avoid. Since the surface of polysilicon is not very smooth, the friction between two structures each made of polysilicon is relatively high. In addition to the friction present, a significant amount of wear is thought to occur as the grains of polysilicon eventually break off. This is thought to cause a polysilicon 'dust' which has been suspected to be linked to the failures of some micromotors [5,6].

To help reduce the friction present in the polysilicon micromotors, techniques such as using silicon nitride to cover the bearing surfaces or as the bearings themselves have been employed [1,8,9]. Since silicon nitride is an insulator, this causes the rotor to be electrically isolated and therefore to have a greater attractive force to the substrate than if the rotor was grounded.

Another method that has been developed and is used for micromotor fabrication is called the LIGA (German for *Lithographie, Galvanoformung, Abformung*) process. The LIGA process was developed in the early 1980's at the Karlsruhe Nuclear Research Center in Germany to enable fabrication of micron-scale devices that could be several times as thick as they are wide. This is a distinct advantage over surface micromachining, which is generally limited to structures whose width and thickness are of the same order. Structures successfully fabricated using LIGA are as narrow as 5 microns, and as thick as 300 microns [7].

The LIGA process typically uses nickel or some other metal as the material for its devices, since the deposition of the material is by electroplating. The motors built by LIGA are sometimes magnetic drive, rather than electrostatic drive that is used by surface micromachined devices. This is possible because of the materials used in the motors.

Since motors fabricated by LIGA require significantly different processing steps (x-ray lithography, electroplating) than those made by surface micromachining, their integration with electronic circuitry on the same substrate becomes difficult. In addition, the availability of synchrotrons to provide the x-rays necessary for the lithography is limited.

This leaves us at the present, where it seems necessary that in order for micromotors to become practical, reliable devices that can be integrated with electronic circuits on a single substrate, advances in designs and/or materials must be made. This thesis concentrates on the latter; namely, using tantalum silicide instead of polysilicon as the rotor/stator and bearing material.

CHAPTER 2

PRINCIPLE OF OPERATION

2.1 Parallel Plate Approximation

In order to understand how the variable capacitance micromotors work, it is first necessary to understand their construction. Figure 2.1a shows a plan view of a typical micromotor with 12 stator poles and 8 rotor poles. Figure 2.1b shows a cross-section of the motor through one of the rotor/stator gaps.

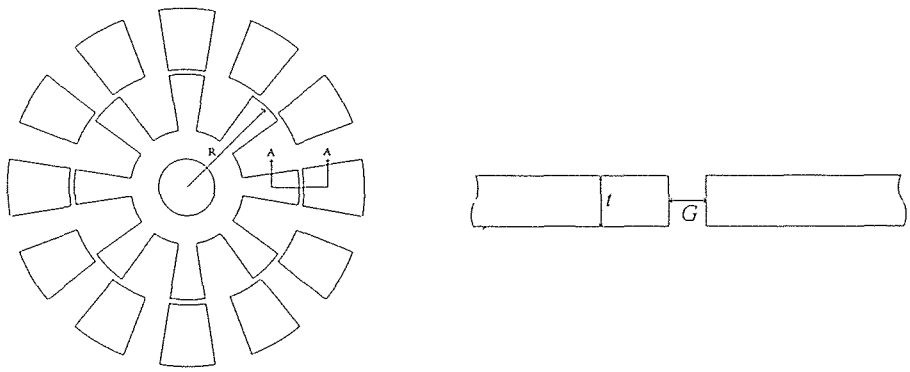

(a) (b)

Figure 2.1 Geometry of a typical micromotor; (a) plan view, and (b) cross-section 'A-A' of rotor/stator gap.

During excitation, one pole of the rotor forms one plate of a parallel plate capacitor, while a stator pole forms the other plate. Neglecting fringing fields (which in this case is not very accurate, but simplifies initial calculations), the rotor/stator capacitance can be expressed as

$$C = \frac{\varepsilon_o \varepsilon_r t R \theta}{G}, \tag{2.1}$$

where ε_O represents the permittivity of free space, ε_r the relative permittivity of the dielectric material in the rotor/stator gap, t the rotor and stator thickness, R the rotor radius, θ the rotor/stator angular overlap, and G the rotor/stator gap. For a typical fabricated motor, the values for these parameters are given in Table 2.1.

Table 2.1 Dimensions of a typical fabricated micromotor.

Parameter	Typical Value
ε_O	8.8542 x 10^{-12} F·m^{-1}
ε_r	1.00059 for air
t	1.6 μm
R	50 μm
G	2.0 μm

Equation 2.1 represents the capacitance for each occurrence of a rotor/stator pole overlap. For the 12:8 stator:rotor pole geometry shown, the number of simultaneous active rotor/stator pole overlapping regions is 4. This corresponds to the number of stator poles divided by the number of phases supplied by the power supply.

In addition to the fringing electric fields, a further complication to the above approximation comes from the vertical offset in the rotor/stator alignment. Due to the specific fabrication method for the micromotor (see Appendix A), the rotor and stator are not perfectly aligned as they are shown in Figure 2.1b. Rather, the plane of the rotor is

slightly lower than that of the stators (see Figure 2.2). This misalignment can be as small as 500Å, or as large as several thousand Angstroms.

Rotor/stator misalignment serves to decrease the effective rotor thickness as it is used in Equation 2.1, since the term t represents one of the linear dimensions of the parallel plate capacitor. Still neglecting fringing fields, the equation must be modified as follows:

$$C = \frac{\varepsilon_o \varepsilon_r t_{eff} R\theta}{G}, \tag{2.2}$$

where t_{eff} represents the *effective* rotor thickness, differing from t by the vertical misalignment of the rotor and stator.

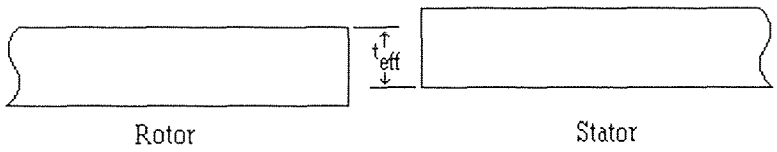

Figure 2.2 Misalignment of rotor and stator due to fabrication method.

By neglecting the fringing fields, the capacitance calculated in equation 2.2 can be significantly smaller than if fringing is considered, depending on the aspect ratio of the rotor and stator thickness to the rotor-stator gap. As expected, a higher aspect ratio means closer correlation to the parallel plate calculation. For an aspect ratio of 4.4, the capacitance calculated taking fringing fields into account is approximately 1.54 times that calculated by the parallel plate approximation. For an aspect ratio of 1.10, the discrepancy is increased to approximately a factor of 2.10 [4].

While the capacitance calculated using the parallel plate approximation is proportional to the aspect ratio, the effect on the fringing fields is not nearly as dependent on the aspect ratio. From a fabrication standpoint, this means that to achieve the best possible motor performance, the aspect ratio of the rotor thickness to rotor-stator gap must be as large as possible. However, due to processing limitations, some compromises must be made between performance and fabrication ease. The significant effect of the fringing fields makes the compromise less costly in terms of motor performance.

2.2 Torque Equations

The expression for the torque applied to the rotor by electrostatic excitation of the stators can be calculated by considering the energy stored in the rotor/stator gap. The energy stored in a capacitor is expressed as

$$W = \frac{1}{2} C V^2, \tag{2.3}$$

where C is the capacitance, and V is the voltage applied across the plates of the capacitor. Assuming a parallel plate capacitor,

$$W = \frac{1}{2} \frac{\varepsilon A}{d} V^2, \tag{2.4}$$

where A is the area of the capacitor plates, and d is the plate separation. Here, ε represents the product of the permittivity of free space and the relative permittivity of the dielectric separating the plates of the capacitor. For the specific case of the micromotor,

$$W = \frac{1}{2}\frac{\varepsilon t R \theta}{G} V^2, \tag{2.5}$$

where t is the rotor and stator thickness, R is the rotor radius, θ is the angular overlap of the rotor and stator, and G is the rotor-stator gap.

By differentiating with respect to θ, the equation for the torque T induced on the rotor is

$$T = \frac{\partial W}{\partial \theta} = \frac{V^2}{2}\frac{\partial}{\partial \theta}\frac{\varepsilon t R \theta}{G}. \tag{2.6}$$

Simplifying,

$$T = \frac{\varepsilon V^2 t R}{2G}. \tag{2.7}$$

Equation 2.7 represents the torque induced on the rotor for each rotor/stator overlap. As indicated previously, for the 12:8 geometry being considered, the number of simultaneously active rotor/stator poles is 4.

Using the values in Table 2.1 and assuming an excitation voltage of 100V, the total maximum torque induced in the rotor is approximately 7.1 pN-m (picoNewton-meter). By taking the fringing fields into account, this number is be multiplied by a factor of approximately 1.5 to 2.1, thereby making it of the same order as those reported in other works [3,4,5,6,10,11].

2.3 Drive Circuit

The design of the micromotor is such that the excitation signal must come from a three phase bipolar power supply. Due to the relatively large frictional forces present in the motor [1,2,3,5,6,8,10,12], it is necessary that the drive circuit be capable of providing in excess of ±100V.

To achieve these requirements, the power supply must consist of 2 separate and distinct sections. The first section is a digital section which creates 6 non-overlapping 0 to 5V square waves from a single clock input. The second section takes these square waves and from each creates one of the six poles of the 3 phase bipolar signal required. Each of the phases can vary from +Vcc to zero to -Vcc, where Vcc can be as high as 300V. The clock, the 6 outputs from the digital section, and the 6 outputs from the high voltage section are shown in Figure 2.3. Notice that in each pair of high voltage outputs (A^+/A^-, B^+/B^-, C^+/C^-), when one of the pair is at +Vcc, the other is at -Vcc. Similarly, when one is at ground, both are at ground.

From a rotational standpoint, the motors would work just as well if a 3 phase unipolar power supply were used instead of the bipolar supply discussed. However, during excitation of the stators, the rotor would tend to charge to the potential of the excited stator poles. Assuming the excitation was positive with respect to ground, this would mean that the rotor would also tend toward a positive potential with respect to ground. This would cause an attractive force between the rotor and the substrate, causing a clamping to occur which would hinder rotation of the rotor. By using a bipolar supply as discussed, this clamping problem is eliminated since opposing stator poles are of opposite polarity (see Figure 2.4), thereby causing the rotor to remain at or near ground potential, minimizing any clamping to the substrate.

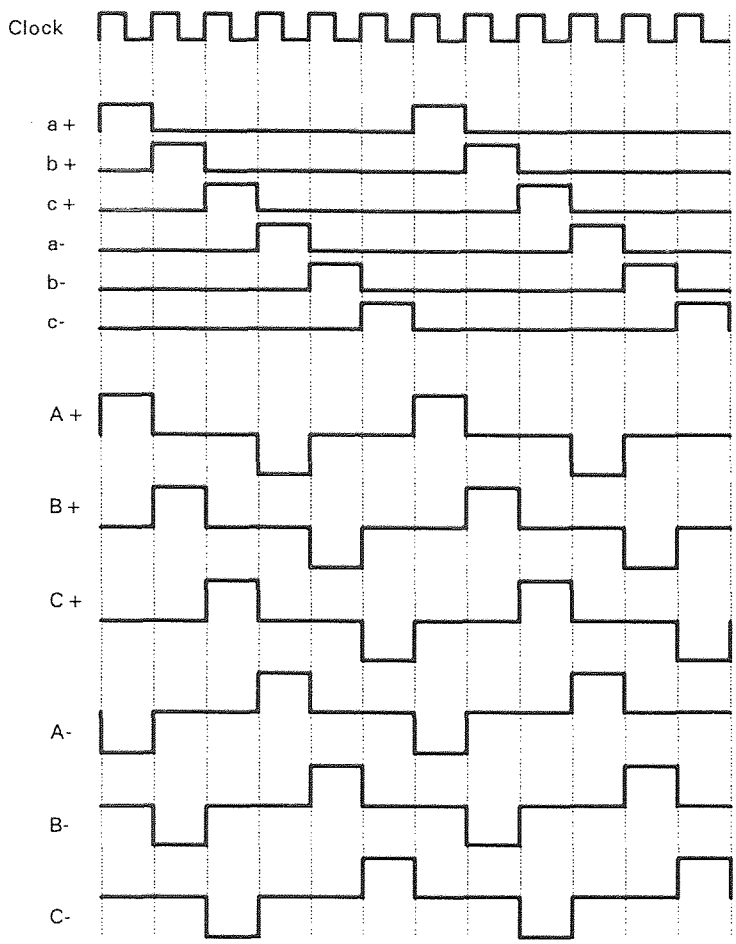

Figure 2.3 Clock signal, 6 digital outputs (a+ to c-), and 6 high voltage outputs (A+ to C-), showing relative phasing of each (amplitude not to scale).

A 3 phase bipolar power supply means that there will be 6 outputs that must be connected to the motor, as well as a ground for the substrate. Again, the benefits of the bipolar supply over the unipolar supply indicate that the added complexity of the supply and of the motor interconnect scheme will be offset by the improved motor performance; since the micromotors are at present of limited reliability, anything that could prove to enhance their performance must be considered very carefully.

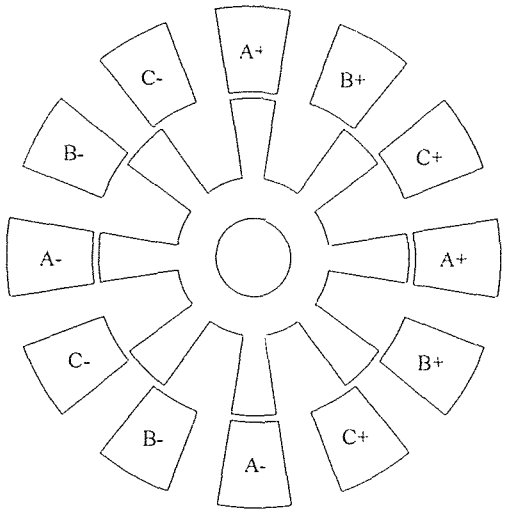

Figure 2.4 Stator pole phasing for the 3 phase bipolar excitation of a 12:8 motor.

CHAPTER 3

MOTOR DESIGN

3.1 Motor Geometry

The basic design of the micromotors is dictated primarily by two things: functionality, and compatibility with standard IC processing techniques. Functionally, the rotor must be free to rotate, unrestricted and with minimum friction, about a center bearing; yet the rotor must be restrained radially as well as axially. Also, the motor must be designed with a means of torque production which is as uniform and as strong as possible.

Compatibility with standard IC processing techniques can be maintained by choosing materials which are themselves compatible, and also by designing the motor in such a way as to ensure that standard processes can be used with little or no modification. The latter of these conditions dictates that the motor be relatively planar in design, and that the dimensions of components be within the limits imposed by current photolithographic and etching processes. Since IC processing does not allow for movable pieces, the motors must be fabricated with the rotors attached to the substrate, and the rotors subsequently released. This means that the rotor must be fabricated on a sacrificial layer, which must then be etched away by a wet chemical process.

In order for the rotors of the motors to be free to rotate, and to be restrained axially and radially, the design of the center bearing must be considered carefully. Two distinct designs for the bearing have been implemented in previous works: the hub design [1,8], and the bearing/bushing design [2-6,9-11]. The hub design uses a single structure for axial and radial restraint of the rotor. Basically, the hub is a circular axle on which the rotor spins, plus two flanges, above and below the rotor, to provide axial restraint (see

Figure 3.1). The bearing/bushing design is incorporated in the designs used in this work, and consists of an axle with only a single flange on top of the rotor, in addition to a number of support pins or bushings on which the rotor rests (see Figure 3.2).

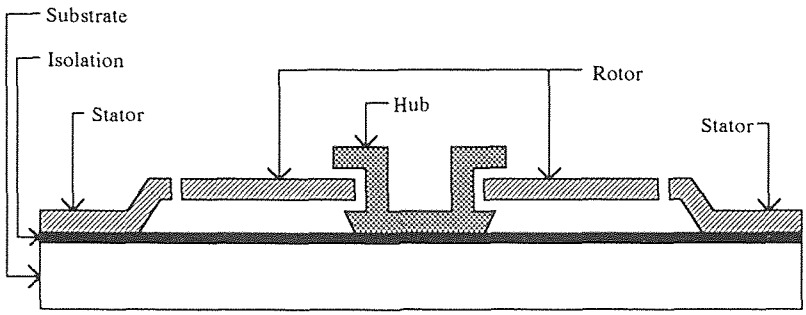

Figure 3.1 Cross section of a motor showing hub bearing design.

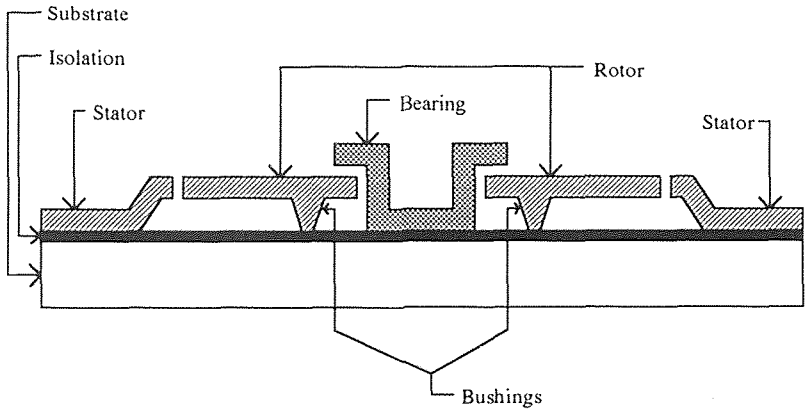

Figure 3.2 Cross section of a motor showing the bearing/bushing design.

The advantage of the bearing/bushing design is that fabrication is simplified since the hub design requires a controlled undercutting of the rotor in the oxide etch and a subsequent oxide deposition to re-establish the gap between the rotor and the hub. The

bearing/bushing design requires only a single timed etch of the oxide to define the bushing molds. Also, the bushing size and location can be easily controlled to provide the minimum friction in the finished device.

The torque in the motors is produced by means of a varying capacitance between the rotor and stator poles. The torque produced is proportional to the angular rate of change of capacitance, as indicated in Equation 2.6. Since the magnitude of the rate of change of capacitance varies as the rotor rotates, the magnitude of torque applied to the rotor also varies. The applied torque is in fact periodic, with a frequency equal to the clock frequency of the drive circuit. In order to minimize the difference between the maximum and minimum torques, simulations of several different rotor/stator geometries were performed in other works [5,6,10,11]. The results of the majority of these analyses indicate that the optimum geometry for the motors includes a stator pole to rotor pole ratio of 3:2, a rotor tooth width to rotor tooth pitch ratio of 0.4, a rotor/stator gap as small as possible, and the rotor pole width equal to the stator pole width [10]. Another proposed optimum geometry is a 24:8 design, with a rotor pole width of 27° and a pitch of 45°, and a stator pole width of 12° and a pitch of 15° [11].

Both of these proposed geometries were included in the mask set used for this work. Several permutations of rotor diameter, rotor-stator gap, rotor-stator pole ratio and number, and bearing and bushing size and type were also included in the mask set. A total of 54 unique motor designs were on each chip, along with several test sites for verifying mechanical and electrical properties of the deposited films. A complete listing of each motor's parameters is given in Appendix C.

3.2 LOCOS Technology

Since the film thicknesses of the materials in the motors are typically on the order of 1μm to 2μm, careful consideration must be given to their design so that photolithographic and etching constraints imposed by standard IC fabrication processes can be adhered to. Two basic variations for the fabrication of the motors have been employed: the so-called 'standard' process, and the LOCOS (LOCal Oxidation of Silicon) process.

The 'standard' process simply uses the silicon substrate as a foundation for a device which is fabricated on top of the substrate. This is the typical design (see Figure 3.3). The first sacrificial oxide layer is deposited on top of a silicon nitride isolation layer and patterned to allow the rotor to be fabricated on top of it, but also to allow the stators to be anchored to the silicon nitride. This oxide is typically 1.5-2.5 μm thick. When the rotor/stator material is deposited over the oxide, the resulting topography is of the same order as the oxide thickness. This creates difficulty in photolithography since in order to cover the topography, the photoresist must be at least as thick as, or thicker than, the oxide. Since the rotor-stator gap should be as small as possible, a problem exists since, as a rule of thumb, the minimum feature that can be patterned in photoresist is approximately equal to the thickness of the photoresist. Since for optimum motor performance the oxide thickness should be maximized while the rotor-stator gap should be minimized, there must be a trade-off due to the difficulty in photolithography to pattern small features over large topographies.

The other option is to utilize LOCOS processing techniques [5] to enhance the planarity of the finished motors (see Figure 3.4). LOCOS involves etching a well, which is defined by a hole in the silicon nitride isolation layer, into the substrate, and subsequently oxidizing the exposed silicon in the well until the oxide is flush with the surface of the silicon nitride. When the rotor/stator material is then deposited, it is virtually flat, thereby minimizing the problem of photoresist coverage over large topographies.

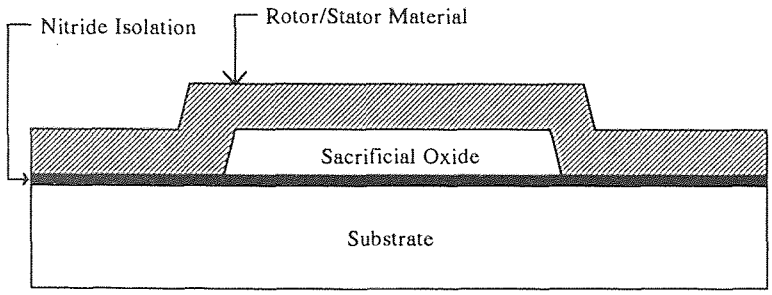

Figure 3.3 Cross section showing large topography of 'standard' process after rotor/stator deposition (not to scale).

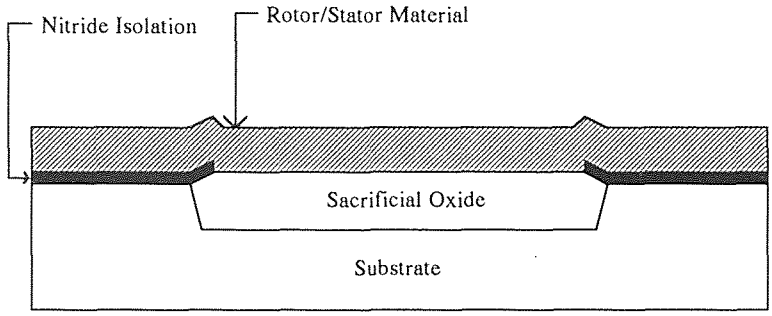

Figure 3.4 Cross section showing relatively planar geometry of LOCOS process after rotor/stator deposition (not to scale).

Clearly the LOCOS process simplifies the subsequent processing steps as well, since the initial oxide step is virtually eliminated. For the standard process, the final photolithography level may have to cover steps as high as 5μm, while with the LOCOS process this number can be reduced by nearly a factor of 2. For a complete set of cross sections of the motors as they are fabricated with the LOCOS process, refer to Appendix A.

3.3 Dimensional Considerations

The dimensions of the micromotors are dictated by the requirements for successful rotation of the motors as well as by processing limitations. Processing limitations refer both to those imposed in order to maintain compatibility with standard IC processing, and also to those which are specific to the fabrication facility being used.

There are several dimensional considerations in reference to optimum performance of the motors. The discussion to follow will proceed in the same order as the issues presented themselves during processing. As each issue is raised, the processing limitations that apply will also be discussed, including both the general limitations relating to maintaining compatibility, and also those specific to NJIT's MRC.

In the LOCOS design, the polysilicon shield plate typically deposited and patterned under the rotor can be eliminated since the rotor will be resting directly on the silicon substrate. The function of this shield plate is to ensure that the rotor is not clamped to the substrate by electrostatic attraction. This is accomplished since the rotor remains in electrical contact with the shield plate through the support pins, thereby assuring that the rotor and shield plate are at the same potential.

Relying on the silicon beneath the rotor to act as a shield plate in devices fabricated with LOCOS requires that the silicon be as conductive as possible. This can be accomplished by performing an ion implant into the silicon during processing [5], or by using a heavily doped substrate to start with. For integration of motors and digital electronics, typically an ion implant would need to be performed, since the requirements of most circuits are that the resistivity of the substrate be on the order of 1-10 Ω-cm. For this work, integration of electronics on the same substrate was not of concern, so a heavily doped substrate was chosen. The resistivity of the starting wafers was less than 0.005 Ω-cm. In addition to relying on the heavily doped substrate, the effect of the shield plate is

further enhanced during LOCOS since the segregation coefficient causes the dopants to remain in the silicon, and therefore to collect at the silicon-silicon dioxide interface.

The thickness of the silicon nitride isolation layer is important since it determines the maximum voltage at which the stators can be biased with respect to the grounded substrate. The silicon nitride used was a PECVD (plasma enhanced chemical vapor deposition) silicon nitride deposited at 600°C and then densified at 850°C. Dielectric breakdown strength of the undensified silicon nitride was measured by patterning a 200 x 220 μm^2 aluminum pad on 1000Å of the silicon nitride, and applying a positive voltage to the pad with the substrate grounded. The average breakdown voltage for 5 points on the wafer was 94V. This translates to a dielectric breakdown strength of 9.4×10^6 V/cm, which is very close to the 10^7 V/cm given for stoichiometric LPCVD silicon nitride [13]. Assuming a maximum stator voltage of approximately 300V, a silicon nitride thickness of approximately 3000Å should be sufficient. Since the silicon nitride etch rate in 49% HF is not zero, some allowance must be made for silicon nitride loss during the release etch. The etch rate of the 850°C annealed silicon nitride was determined to be approximately 90 Å/min in 49% HF. Allowing for approximately 20 minutes of release time, the silicon nitride thickness must be increased by approximately 2000Å, for a thickness of approximately 5000Å. The target thickness for the silicon nitride deposition was set at 5400Å, which allowed for some processing latitude in the silicon nitride thickness. The as-deposited thickness of the silicon nitride was approximately 5100Å.

The thickness of the LOCOS oxide determines the maximum possible separation of the rotor and the substrate. This dimension is important since the attractive force between the rotor and substrate for a given induced charge on the rotor is inversely proportional to their separation (this is assuming that the rotor and substrate shield are not in perfect electrical contact). This means that for optimum motor performance, the oxide should be as thick as possible. However, growing a thick thermal oxide is very time consuming. For a 12 hour oxidation in NJIT's wet thermal oxidation furnace, the oxide thickness is

approximately 1.45μm. The nature of thermal oxidation is such that the rate of growth slows as the oxide grows thicker, since the diffusion time of the oxygen through the existing SiO_2 increases with oxide thickness. In order to increase the oxide thickness to 2.0μm, the time would need to be increased to approximately 25 hours. For this reason, it was decided that 1.45μm would be satisfactory, at least for the initial trials.

The support pin height is defined by etching molds into the LOCOS oxide. The maximum height of the support pins is limited by the thickness of the oxide, but must be made slightly less so that when the rotor material is deposited, there is still a thin film of oxide left between it and the substrate below. This ensures that when the rotors are released, they are not attached to the substrate by the support pins. Since the support pin molds are not etched completely through the oxide, the rotor ends up lower than the stators, as shown in Figure 2.2. These two conditions indicate that the support pin molds should be etched as far through the oxide as possible without risking penetration to the substrate below. The etch performed is a timed etch in 7:1 BOE (buffered oxide etch, 7 parts 49% ammonium fluoride, 1 part 49% HF), in which the etch rate of oxide is determined with a control wafer immediately prior to the support pin mold etch. The support pin molds were etched approximately 90% through the oxide, leaving less than 2000Å oxide at the bottom of the molds.

The thickness of the rotor and stator material is important from an electrical standpoint as well as a mechanical standpoint. Mechanically, the rotor must be rigid enough not to bend or warp when released. Electrically, the rotor and stators should be as thick as possible to maximize the torque produced in the motors (see Equation 2.7), since the torque is proportional to the thickness (neglecting fringing fields). Also important in maximizing torque is the gap between the rotor and stators. As seen in Equation 2.7, the torque is inversely proportional to the rotor/stator gap (again neglecting fringing fields). From a processing standpoint, these two parameters are not independent. In general, photolithography and etching limitations mean that if one of these parameters increases,

the other also will. Since the LOCOS process enhances the planarity of the motors, the photolithography is simplified. If the standard non-LOCOS process had been used, the step coverage of the photoresist at the rotor-stator etch level would need to have been on the order of 1.5 - 2.0μm (the thickness of the sacrificial oxide). In addition to the step coverage required, the thickness of the photoresist would have to be further increased so that after the rotor/stator etch the remaining photoresist would still cover the rotor. Assuming a selectivity of resist to tantalum silicide during the plasma etch of approximately 10:1, this would mean approximately an additional 2000Å of photoresist. Because the LOCOS process is planar at this level, a thinner photoresist could be used (1.2 - 1.5μm), meaning a potentially smaller rotor/stator gap. From an etching standpoint, the degree of anisotropy of the etch process determines the maximum thickness of the rotor/stator material and the minimum rotor/stator gap. The thickness of the rotor/stator material chosen for this work was 1.5 - 1.6μm. The data used to make this decision will be discussed in Chapters 4 and 5.

The second sacrificial layer was a low temperature oxide (LTO) deposited by chemical vapor deposition (CVD) over the rotor and stators. The thickness of the LTO, in particular its sidewall thickness, determines the bearing clearance in the finished device. For this reason, it was necessary that the LTO thickness be less than the minimum rotor-stator gap, since the rotor is able to move laterally from center a distance equal to the thickness of the LTO. The thickness of the LTO also determines the gap left between the stator interconnects which are patterned in the second tantalum silicide. This gap should be maximized so that dielectric breakdown does not occur between the stator and the overhanging interconnect. The LTO thickness for the devices was 5000Å, half of the minimum rotor/stator gap.

CHAPTER 4

FABRICATION

All of the fabrication work for this thesis, with the exception of the silicon nitride deposition and the LTO deposition, was performed at the NJIT Microelectronics Research Center (NJIT MRC). The starting substrates were 5", <100> n-type (As) silicon wafers, resistivity < 0.005 Ω-cm. A detailed process sequence can be found in Appendix A.

The process was a two-level tantalum silicide ($TaSi_2$) process, with silicon nitride used for the stator/substrate isolation, thermally grown silicon dioxide (oxide) as the first sacrificial layer, and LTO as the second sacrificial layer. As fabricated, the micromotors are 5 mask devices: NITRIDE1, OXIDE1, POLY1, OXIDE2, and POLY2 (the POLY masks are used to pattern the tantalum silicide).

4.1 Silicon Nitride Deposition and Patterning

The silicon nitride used for this device was a PECVD silicon nitride obtained from the Army Research Laboratory, Ft. Monmouth, NJ. Before deciding to use the standard silicon nitride process available at Ft. Monmouth, two important characteristics needed to be determined. First, the etch rate of the silicon nitride in 49% HF was measured to determine the silicon nitride's ability to withstand the release etch which would be the final step in the fabrication process. Next, the dielectric breakdown strength was measured to determine the thickness necessary for stator-substrate isolation.

Initial measurements of etch rate showed that the standard silicon nitride process was not suitable. The etch rate of the standard silicon nitride in 49% HF was

approximately 1500Å/min. Assuming a minimum release time of 5 minutes, the amount of silicon nitride consumed would be approximately 7000Å. Allowing an additional 3000Å to be left to withstand the voltage applied to the stators, the silicon nitride would have to be deposited at 10,000Å. This would be problematic from an etching standpoint, since the silicon nitride etch used is isotropic; the undercutting of the photoresist during such a long etch would increase feature sizes by nearly 2μm. Stress in the silicon nitride at this thickness did not seem to be a problem, probably because it was deposited by PECVD at low temperature, a process that typically produces low stress films [16].

By increasing the deposition temperature from 380°C to 600°C (the maximum temperature capability of the system), the etch rate of the silicon nitride in 49% HF was decreased from 1500Å/min to 275Å/min. By densifying the silicon nitride for 1 hour at 850°C under nitrogen, the etch rate was further decreased to 90Å/min. This was the final process chosen for the silicon nitride deposition. The deposition parameters are shown in Table 4.1.

Table 4.1 Silicon nitride deposition parameters.

Parameter	Value
SiH_4 flow	470 sccm
NH_3 flow	3.8 SLM
Pressure	2 Torr
Temperature	600°C
Power	1375 Watts
Duty Cycle	32 msec ON 280 msec OFF
Deposition Rate	120 Å/minute
Post-Deposition Densification Temperature/Time	850°C/1 hour

The second important characteristic of the silicon nitride is the dielectric breakdown strength, the measurement of which was discussed in Chapter 3. The breakdown strength of the silicon nitride was determined to be 9.4 x 10^6 V/cm. As was also discussed in Chapter 3, the as-deposited thickness of the silicon nitride was 5100Å.

The next step was photolithography for the NITRIDE1 mask level. NJIT's standard photolithography process was used. A summary of the coat, bake, and develop conditions is given in Table 4.2.

The silicon nitride etch was done in a Drytek DRIE-100 plasma etcher. The geometry of the etcher is such that 6 wafers can be etched simultaneously between 6 pairs of parallel plate electrodes. The initial trials to determine optimum etch conditions utilized sulfur hexafluoride (SF_6) as the etchant gas [14]. Several experiments showed that after 3-5 minutes of etching, a hazy film formed on the surface of the test wafer. The film was impervious to HF, BOE, and 5:1 sulfuric peroxide (5 parts H_2SO_4, 1 part 35% H_2O_2), as well as to an O_2 plasma. An etch chemistry of 92% Freon 14 (CF_4) and 8% O_2 was then tried [15]. This etch produced no haze on the wafer, and the etch rate was acceptable. A summary of the etch parameters is given in Table 4.3.

Table 4.2 NJIT's standard photolithography process.

Parameter	Value
Vapor HMDS Temperature	135°C
Photoresist	Shipley 3813
Spin Speed	4500 RPM
Spin Time	25 seconds
Soft Bake Time/Temperature	60 seconds/110°C
Exposure Power Density	25 mW/cm^2
Developer	Shipley MF 319
Develop Time	45 seconds
Hard Bake Time/Temperature	60 seconds/115°C

Since the CF_4/O_2 plasma etches silicon faster than silicon nitride, and since the Drytek etcher doesn't have a satisfactory end point detector, it was necessary to control the etch time of the silicon nitride precisely. For this reason, the silicon nitride thickness was measured individually on each wafer. The wafers were then etched for 10 minutes (slightly less time than required to etch all the silicon nitride). Compensating for the etch rate of the photoresist, a step profiler was used to determine the depth of the etched cavities in the silicon nitride. Comparing this number to the original silicon nitride thickness allowed a precise calculation of the etch rate of the silicon nitride on each individual wafer, and therefore enabled a calculation of the additional time required to complete the etch of the silicon nitride. All of these measurements and calculations were carried out independently for each wafer processed.

Before the photoresist was removed, a cavity, coincident with that etched in the silicon nitride, needed to be etched into the substrate so that the LOCOS oxide, when grown to a pre-determined thickness, would be planar with the top surface of the silicon nitride. The details of this process will be discussed in the next section.

Table 4.3 Silicon nitride plasma etch parameters.

Parameter	Value
CF_4 flow	92 sccm
O_2 flow	8 sccm
Pressure	250 mTorr
Power	600 Watts
Temperature	35°C
Etch Rate	485 Å/min

4.2 LOCOS Oxide Surface Planarization

In order for the surface of the LOCOS oxide to be planar with the top surface of the silicon nitride, the thickness of the oxide and the depth of the cavity etched into the substrate subsequent to the silicon nitride etch must both be controlled very carefully. Since the LOCOS oxide is a wet thermal oxide, some of the silicon substrate was consumed during the oxidation. To be more precise, a thermal oxide grows 56% from the original silicon surface, and consumes 44% of its thickness of silicon [16]. For a desired oxide thickness of 1.5μm, and a silicon nitride thickness of 5100Å, the depth of the silicon cavity needed was 3300Å.

The silicon etch was carried out in the same Drytek plasma etcher. In fact, the etcher is such that up to 3 individual etching processes can be run sequentially. This enabled the etching of the silicon to be done immediately after the silicon nitride finishing etch, without venting the etch chamber. The silicon etch conditions are given in Table 4.4.

Table 4.4 Silicon plasma etch parameters

Parameter	Value
SF_6 flow	15 sccm
C_2ClF_5 flow	25 sccm
Pressure	200 mTorr
Power	400 Watts
Temperature	25°C
Etch Rate	2450 Å/min

After the silicon nitride finishing etch (wafer specific times), the silicon substrate was etched for 80 seconds. The photoresist was then removed in 5:1 sulfuric peroxide and the total depth of the cavities was measured with a step profiler. For a lot of 8 wafers, the mean depth of the cavity was 7960Å, with a range of 7850Å to 8140Å. Based on this number (slightly less than the 8400Å target), and based on the oxidation thickness vs. time curves for NJIT's wet thermal oxide, the oxidation time needed was calculated to be 12 hours. The oxidation parameters are shown in Table 4.5.

Table 4.5 Wet thermal oxidation parameters

Parameter	Value
Tube Temperature	1000°C
Bubbler Temperature	98°C
Tube Oxygen Flow	2 SLM
Bubbler Oxygen Flow	750 sccm

Since a 12 hour oxidation requires approximately 14 hours (including the temperature ramp and stabilization times), it was decided to perform two oxidations. Since the purpose of the oxide is for a sacrificial layer only, the oxide quality was not important. The fact that two successive oxidations would probably create an intra-oxide interface which would be undesirable for any other application was not of concern for this device since the electrical properties of the oxide were not important. The oxidation was therefore performed as two 6 hour oxidations, with the wafers remaining at 500°C under nitrogen between oxidations.

A control wafer was added to the lot prior to oxidation so that oxide thickness could be accurately measured (since the oxide grew only in the small windows opened

through the silicon nitride on the device wafers, oxide thickness measurements were difficult). The oxide thickness on the control wafer was measured at the 6 hour mark to verify that the oxide thickness was as expected. The established thickness vs. time curves proved to be accurate to within 1 percent.

The oxide thickness on the control wafer was measured after 12 hours of oxidation, also. The mean thickness was 14545Å, with a range of 14463Å to 14606Å. The height of the oxide relative to the silicon nitride surface was measured on the device wafers. The oxide was slightly higher than the silicon nitride, by 150Å to 530Å. These numbers would change slightly before the rotor/stator material deposition, since the next step was to remove any oxy-nitride that may have formed on the silicon nitride surface during the long oxidation process. This was accomplished with a 5 minute etch in 100:1 H_2O:HF. Since the etch rate of the oxide in 100:1 H_2O:HF was approximately 100Å/min, the worst case would be where no oxy-nitride was removed, thus reducing the oxide thickness by about 500Å. The oxide then would be planar to approximately 350Å below the silicon nitride surface, still an acceptably planar surface.

4.3 Timed Etch of Support Pin Molds

After completion of the LOCOS oxidation, molds for the rotor support pins were etched into the oxide. The diameter of the pins on the mask is 3μm. The etch was a timed wet etch in 7:1 BOE. Immediately prior to the etch, the etch rate of thermal oxide was measured so that precise control of the depth of the molds could be achieved.

To ensure that no oxide remained on the backside of the wafers after the support pin mold etch (necessary to enable backside contact to the substrate), the fronts of the wafers were coated with photoresist and the backsides etched for 15 minutes in 7:1 BOE.

This didn't remove all the backside oxide, but the remaining oxide was thin enough that removal would be complete after the support pin etch.

The etch time of the support pin molds needed to be accurately controlled to ensure that the molds were as deep as possible without breaking through the oxide and contacting the underlying substrate. The support pins should be as long as possible so that the fringing field of the rotor to stator capacitor can be as large as possible without interference from the grounded substrate, and so that if there is poor electrical contact between the rotor and substrate, the clamping force between the rotor and substrate would be minimized. If the molds were to penetrate through to the substrate, the rotor would become fused to the substrate and would not be free to move.

To etch the support pin molds, 1.2μm of photoresist was applied and patterned. To determine etch rate of the thermal oxide, as well as to ensure good photoresist adhesion during the long etch of the oxide, the etch was done in two steps. First, the oxide was etched for 8 minutes in 7:1 BOE. The remaining thickness of the oxide was then measured on the control wafer to determine etch rate. The measurement indicated that an additional 9.5 minutes was required to achieve the desired depth of the support pin molds.

At the midpoint pause in the etch, the photoresist was rebaked to increase adhesion to the oxide. Even with this added precaution, there was still some evidence of the photoresist lifting around the support pin molds. The circles around the support pin molds in Figure 4.1a indicate BOE undercutting the photoresist and etching the oxide slightly. The circles varied in size, and did not appear at all the support pin locations on the wafer. Figure 4.1b shows a cross section of what the support pin molds probably looked like as a result of the BOE undercutting the photoresist.

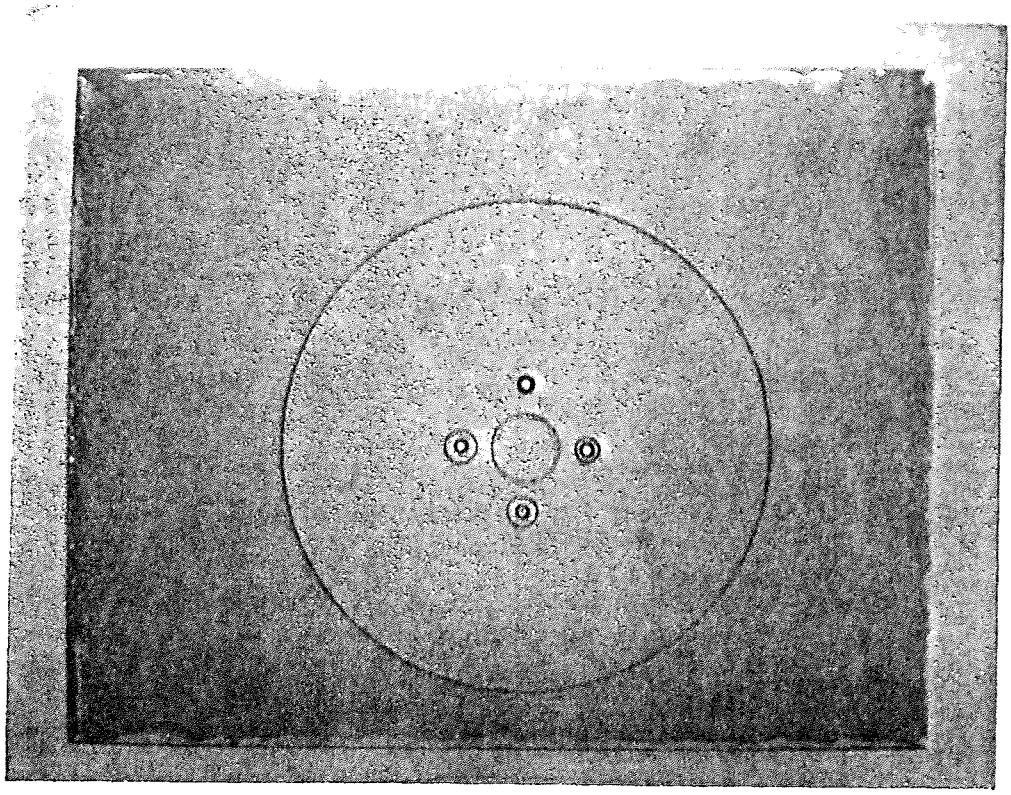

(a)

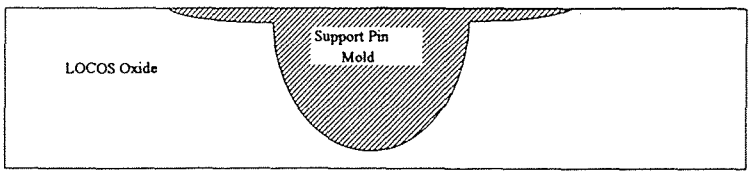

(b)

Figure 4.1 (a) Optical micrograph showing circles around support pin molds in LOCOS oxide, and (b) theoretical cross-section of support pin molds showing result of BOE undercutting the photoresist.

The thickness of the oxide remaining on the control wafer was approximately 200 to 300Å. Since the etch rate of the oxide would be faster on the control wafer than it would be in the 3μm diameter holes on the device wafers (due to the increased transit time of the BOE from the bulk of the etchant down through the holes and to the silicon dioxide surface), the thickness of the oxide remaining at the bottom of the support pin molds was assumed to be greater than this, although measurement was not possible with the equipment available at that time at NJIT's MRC.

4.4 First Tantalum Silicide Deposition and Patterning

Deposition and patterning of the rotor/stator layer followed the support pin mold etch. Tantalum silicide was used for the rotor and stator material, and was obtained by sputtering from a composite target in a Varian 3125 magnetron sputtering system. The deposition parameters are given in Table 4.6.

Table 4.6 Deposition parameters for tantalum silicide

Parameter	Value
Deposition Temperature	300°C*
Base Pressure	8.0×10^{-7} Torr
Deposition Pressure / Backfill Gas	3 mTorr / Argon
Deposition Rate	3 Å/second
Target Composition	$TaSi_{2.4}$

*The substrates are heated to 300°C prior to deposition; the heaters are then turned off.

The one significant problem that manifested itself in the deposition of tantalum silicide was that the stress in the deposited tantalum silicide would cause small pieces to occasionally flake off of the S-gun in the sputtering system and disrupt the plasma over the target. Sometimes, the flakes would cause shorting of the anode to the target (which was grounded), causing the plasma to be lost. Because the power applied to the plasma is controlled through a feedback loop with a deposition rate monitor, the power called for by the deposition controller would begin to increase, since when the plasma was disrupted, the deposition rate began to drop off toward zero. When this occurred, the increased power was enough to quickly melt the small flake of tantalum silicide which caused the short in the first place. When the flake melted, the plasma would be restored, but at a significantly higher power than desired. The sudden burst of power would usually result in loss of the plasma again. After this cycle repeated 2 or 3 times, the machine would abort the deposition.

Two things were ultimately done to remedy this problem. First, the maximum power for which the deposition controller could call was limited to 1 - 2% higher than that required to maintain the desired deposition rate. This meant that if there was a short in the plasma, the power level at which it came back on when the flake finally burned up was not significantly higher than where it should have been to maintain the desired deposition rate. The second was that the deposition rate was lowered from 10 Å/second to 3 Å/second. This seemed to reduce the amount of flaking that occurred in the deposition chamber, which allowed deposition of up to 3.3μm of tantalum silicide (thicker films probably would have worked, too; there was never any need for them, though) with no flaking problems during deposition. When the chamber was vented to unload the wafers (necessary since the Varian 3125 is a batch system), a significant amount of flaking of tantalum silicide occurred from the areas of the chamber closest to the S-gun.

One of the justifications for using tantalum silicide instead of polysilicon as the primary microelectromechanical material for the micromotor is that the surface of

tantalum silicide is typically much smoother and less grainy than that of LPCVD polysilicon. Figure 4.2 shows two optical micrographs; (a) is a view of approximately 2.5 μm of LPCVD polysilicon deposited over the LOCOS oxide cavity, and (b) is the same view with approximately 1.6μm of tantalum silicide substituted for polysilicon. Though the polysilicon is thicker than the tantalum silicide in these micrographs, it was observed qualitatively that the surface of tantalum silicide of up to 3μm thick remained as smooth as the underlying substrate.

Typically, after tantalum silicide is deposited, the next step is to sinter it at high temperature (900 - 1000°C) [17]. High temperature sintering, or annealing, is desired in order to decrease the resistivity of the film. For films deposited at NJIT's MRC, the as-deposited resistivity was approximately 230μΩ-cm. After sintering at 900°C for 30 minutes, the resistivity dropped to approximately 80μΩ-cm. This is very close to other experimental values [17], but slightly higher than that given in literature [13,16,23].

For the thick films required for these devices, however, high temperature annealing was not possible due to the stress developed in the films during the anneal. Attempts to anneal the tantalum silicide at temperatures above the deposition temperature of 300°C proved detrimental to the integrity of the film. In all cases, one, or sometimes both of the following would occur: either the tantalum silicide would form micro-cracks bordered by significantly larger cracks that were visible to the naked eye, or it would peel off of the substrate. Figure 4.3 shows a micrograph from a scanning electron microscope (SEM) of one of the contact pads of the motor suspended above the substrate only by the 12μm wide stator connection. Evident is the concordial fracture of the silicon substrate where the pad used to be. The depth of the fracture cavity was approximately 5μm.

Several sintering processes were tried for the thick tantalum silicide films to attempt to minimize the stress developed in the film. Different sintering temperatures, as well as long and short temperature ramps, were tried. However, the temperature ramps did not seem to be important in determining stress in the tantalum silicide. Once the

temperature reaches 900°C, the cooling of tantalum silicide on a silicon substrate results in a room temperature tensile stress of approximately 8 x 10^8 Pa, regardless of cooling time. Any further temperature treatment of the film does not change the room temperature stress in the film [17].

By keeping the thickness of the tantalum silicide below approximately 7000Å, stress as a result of annealing at 950°C was not a problem. However, for the micromotors to operate well, it is necessary for the rotor and stators to be as thick as possible in order to maximize the capacitance between them. Since the processes previously run by MIT and UC Berkeley used rotor thicknesses on the order of 2μm, it was decided to follow those guidelines for this device. The final thickness used for the rotor and stators was 1.6 μm, with all subsequent processing done at or below 300°C in order to minimize the problems caused by stress. This means that the tantalum silicide did not undergo the crystallization that occurs at high temperature; it is therefore believed that the material on the device wafers was amorphous $TaSi_{2.4}$, the same as is in the sputtering target.

The thickness of the tantalum silicide was decided upon based partly on the ability to successfully etch it anisotropically. The etch recipe used is given in Table 4.7. The degree of anisotropy of the etch was slightly less than one, and the selectivity to photoresist was on the order of 2:1. By limiting the thickness of the tantalum silicide to 1.6μm, these factors were less important than if the tantalum silicide was thicker.

Because of the planar surface on which the tantalum silicide was deposited, the surface of the tantalum silicide was planar as well. This meant that photolithography for this level (the most critical level of the motors - that in which the rotor and stators are patterned with a 1μm gap between them) was relatively simple; NJIT's standard 1.25μm coating of photoresist could be used. The tantalum silicide was etched for 50 minutes, then the photoresist removed in 5:1 sulfuric peroxide. An optical micrograph of the etched tantalum silicide is shown in Figure 4.4.

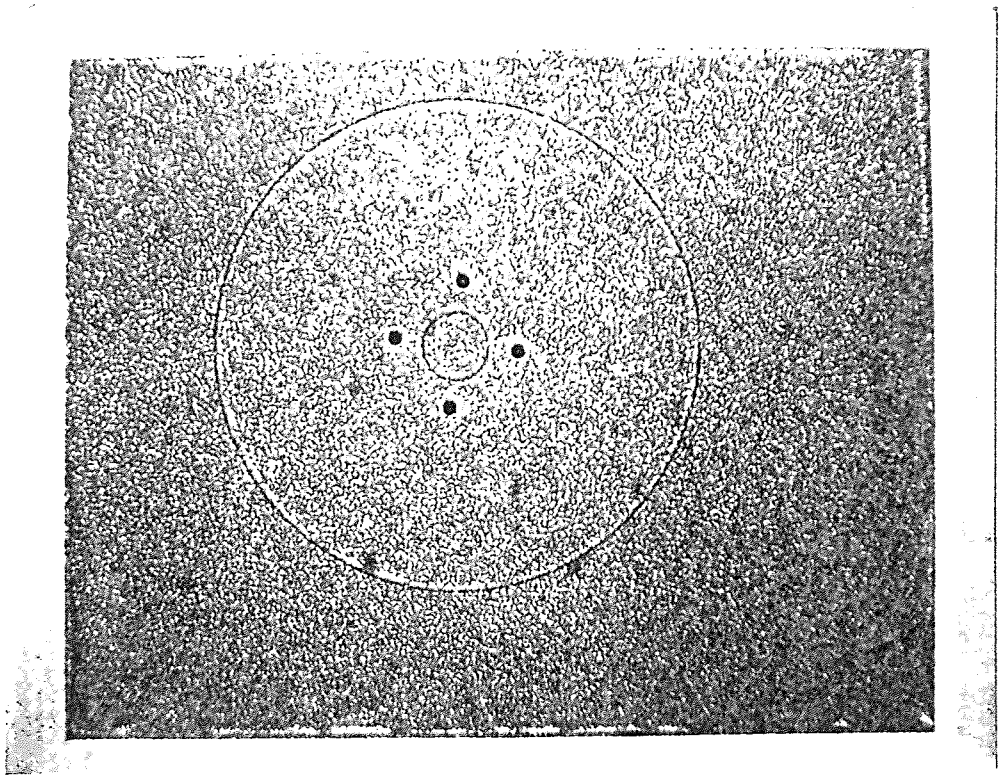

(a)

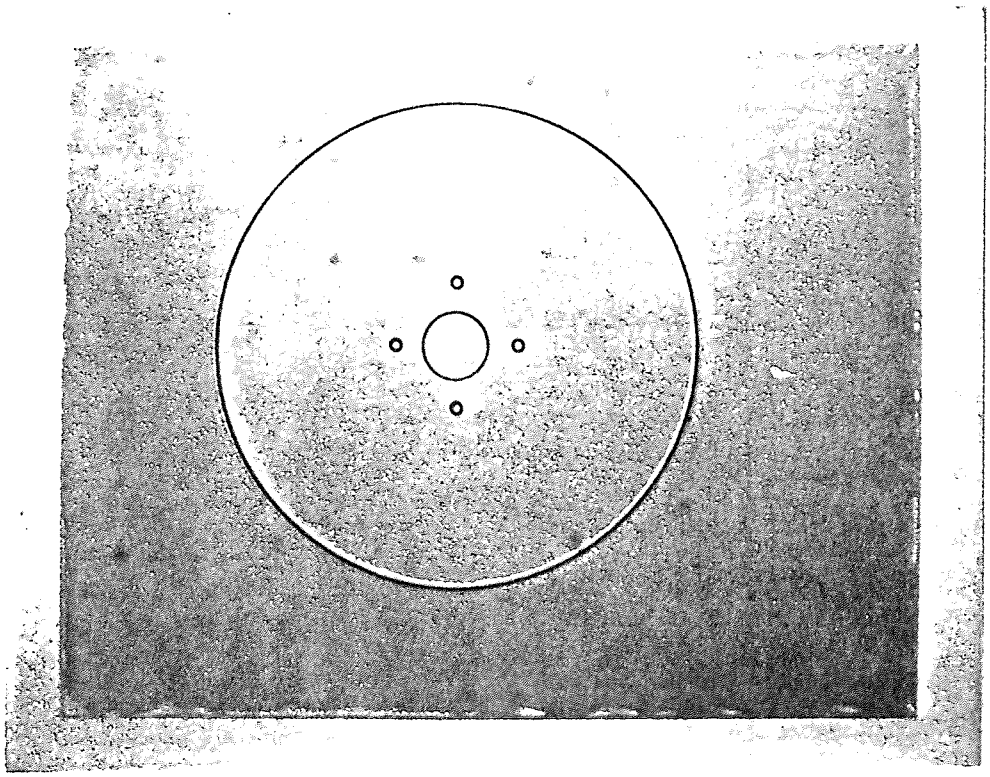

(b)

Figure 4.2 Optical micrograph of the surface of (a) polysilicon, and (b) tantalum silicide.

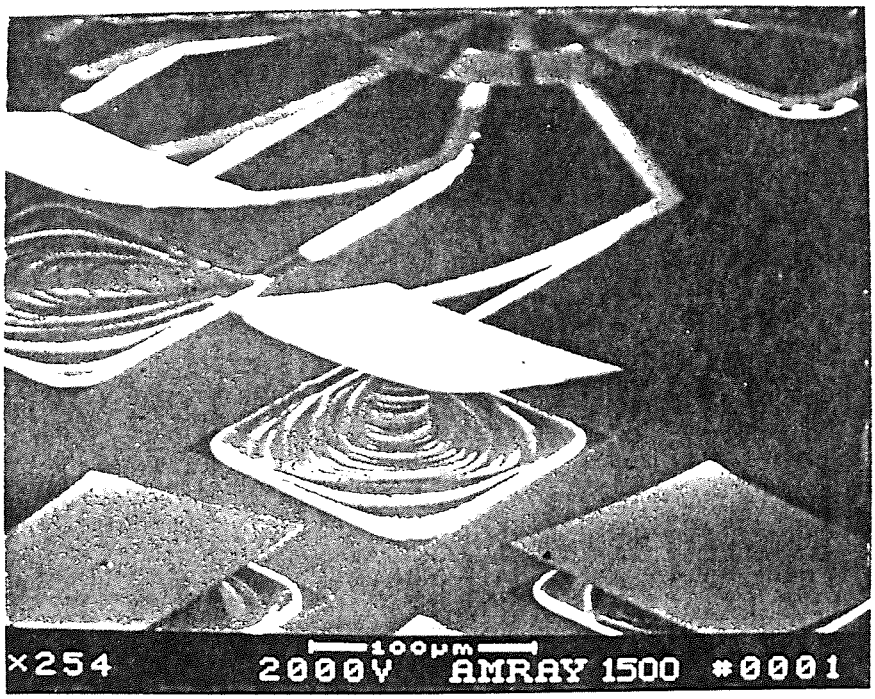

Figure 4.3 Scanning electron micrograph of concordial fracture of silicon substrate due to the stress-related lift-off of a tantalum silicide bonding pad.

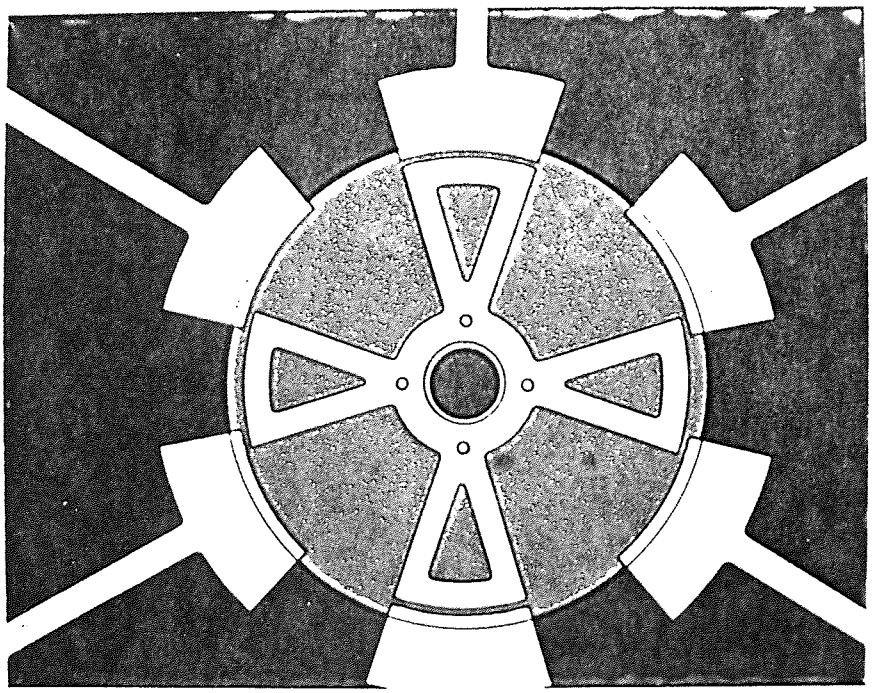

Figure 4.4 Optical micrograph of a 150µm motor after rotor and stator etch.

Table 4.7 Plasma etch parameters for tantalum silicide.

Parameter	Value
SF_6 flow	25 sccm
C_2ClF_5 (Freon 115) flow	75 sccm
Pressure	150 mTorr
Power	600 Watts
Temperature	10°C
Etch Rate	320 Å/minute

4.5 LTO Deposition and Patterning

In order to create the bearing clearance in the micromotor, a layer of LTO was deposited over the rotor and stators. The basic requirements for this LTO were that it be conformal, so that the side walls of the rotor would be completely covered to provide the necessary lateral bearing clearance, and that the deposition temperature be no higher than 300°C in order to prevent stress related failure of the tantalum silicide previously deposited and patterned.

Since at the time of fabrication of this device NJIT's LPCVD LTO process was not operational, it was necessary to find an alternate source of LTO. The LTO used was a PECVD LTO, deposited at 300°C. The final thickness of the LTO was 5000Å. This thickness provided the required separation between the rotor and the subsequent bearing, and also was thin enough that the maximum allowed rotor movement was less than the rotor/stator gap, thereby preventing the rotor and stators from being able to short together. Although PECVD depositions are typically not as conformal as LPCVD, the requirement that the deposition be carried out at a maximum temperature of 300°C limited the choice of processes that could be used.

The photolithography at this level became somewhat more difficult than at the previous levels, since the photoresist was required to cover steps as high as 1.6μm (the thickness of the tantalum silicide rotor and stators). For this reason, the photoresist thickness was increased to 2.1μm. The LTO was etched in 7:1 BOE for 2 minutes. An optical micrograph of the motor after the LTO etch is shown in Figure 4.5.

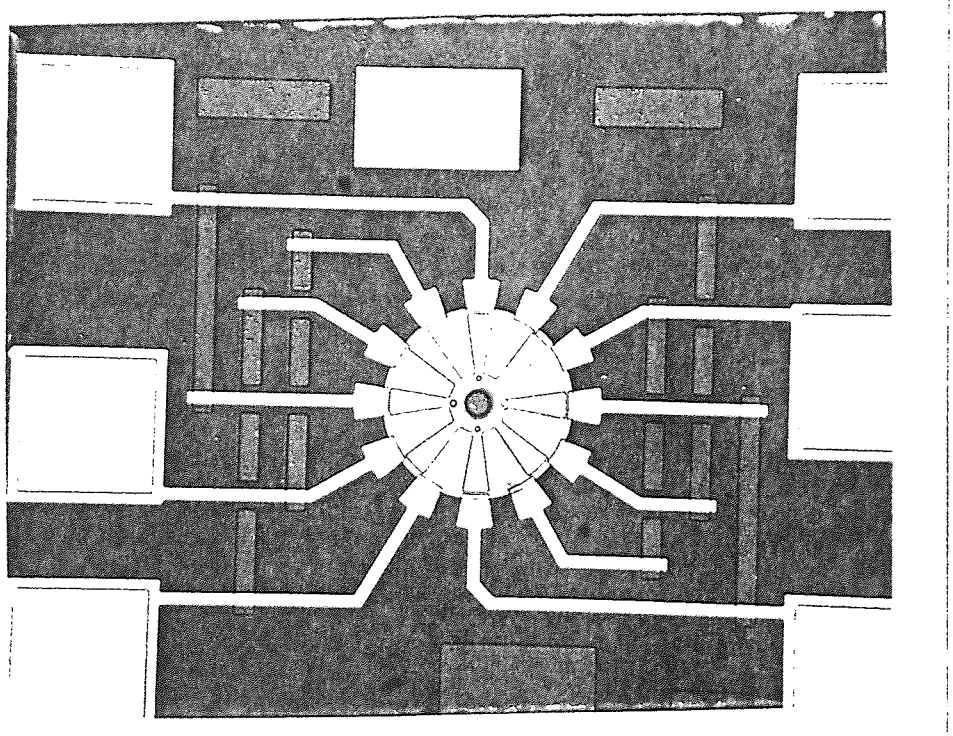

Figure 4.5 Optical micrograph showing a micromotor after the LTO etch.

4.6 Second Tantalum Silicide

For the bearing, 1μm of tantalum silicide was deposited and patterned using the same deposition conditions and plasma etch parameters used for the rotor and stators. Since the steps present on the wafer at this level were approximately 2.1μm, a 2.6μm photoresist

was used. The plasma etch time required for the tantalum silicide was 38 minutes. Figure 4.6 shows a complete, unreleased micromotor.

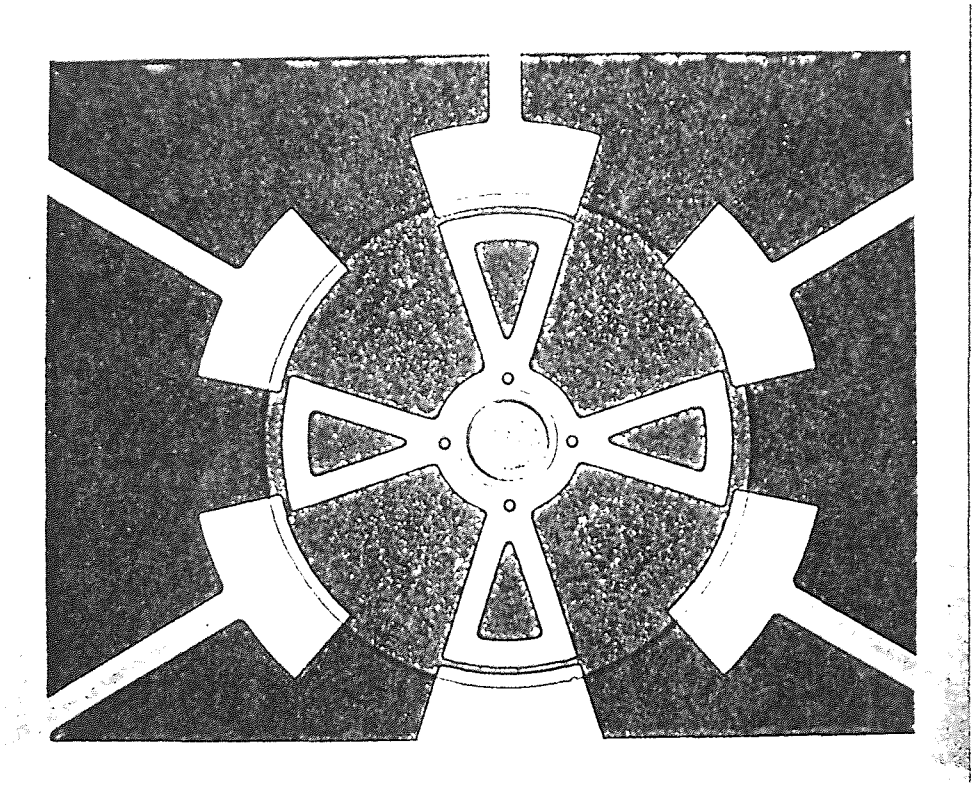

Figure 4.6 Optical micrograph of a complete, unreleased micromotor.

4.7 Sacrificial Oxide Release Etch

The final process step in the micromotor fabrication was to release the rotors by removing the sacrificial layers of silicon dioxide. The complete unreleased motors were etched in 49% HF for 5 minutes. Assuming an etch rate of the thermal oxide of approximately 1.5μm/minute, the 10μm wide rotor poles would be completely released. Some of the

larger rotors would require more time, but for the initial trial, releasing some of the rotors was all that was desired.

After the 5 minute etch and subsequent rinse and dry, the motors were inspected. It was found that the second tantalum silicide layer was completely gone; either etched away or lifted off. Also, the ends of the stators, which overhang the LOCOS oxide well, were gone. Several of the test features on the chip were also damaged.

Another set of motors was etched in 7:1 BOE for 80 minutes. Similar results were observed as for the motors released in 49% HF. Optical micrographs of the released motors are shown in Figures 4.7 and 4.8. At this point, the motors have not yet been successfully released. A more detailed discussion of tantalum silicide's solubility in HF solutions will be given in Chapter 5.

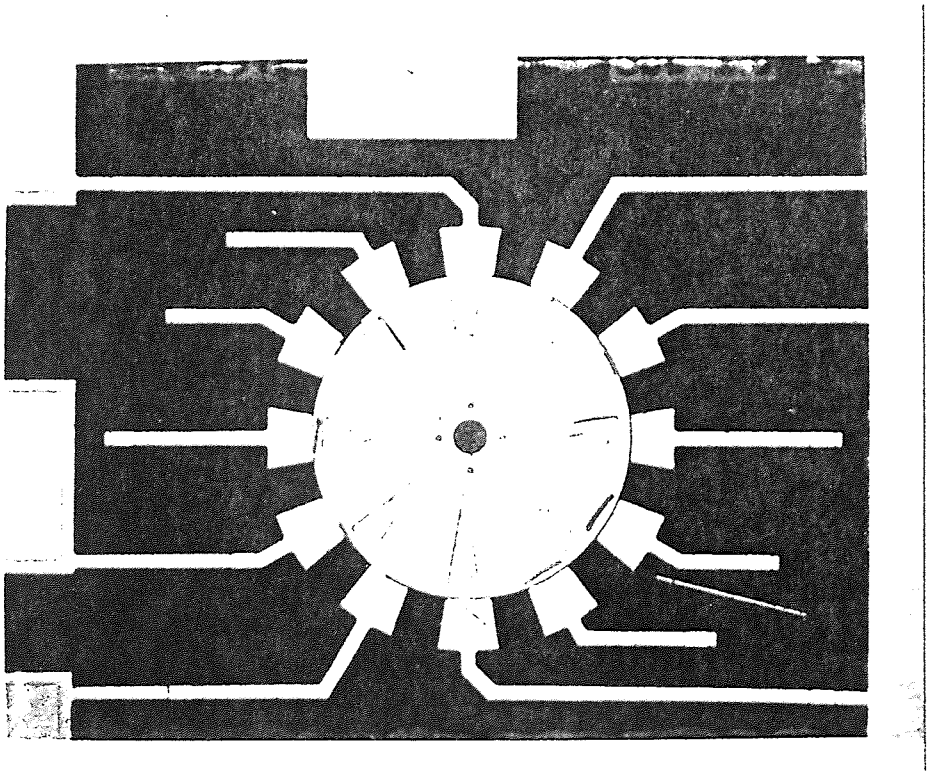

Figure 4.7 Optical micrograph showing a motor released for 5 minutes in 49% HF.

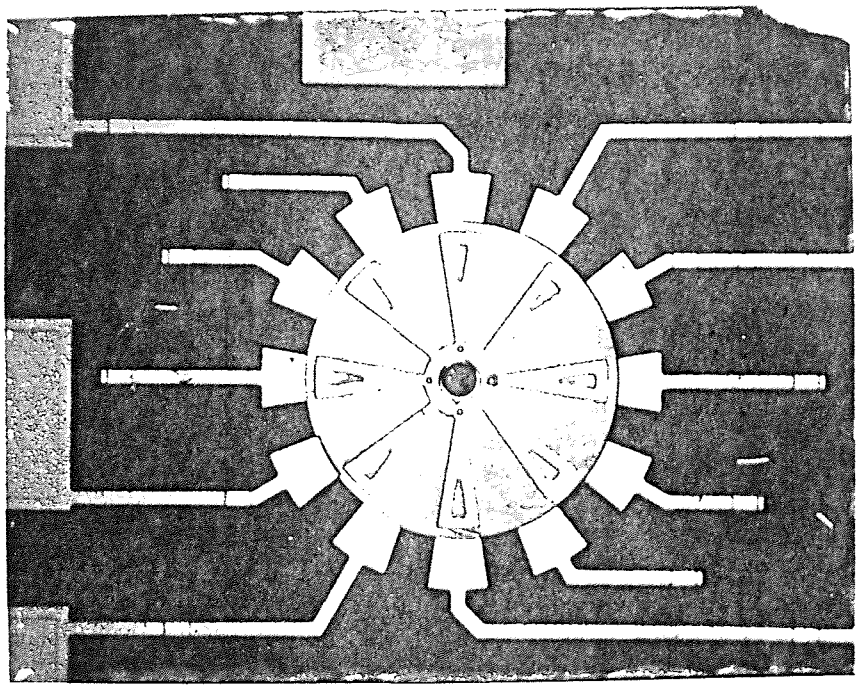

Figure 4.8 Optical micrograph of a motor released for 80 minutes in 7:1 BOE.

CHAPTER 5

PROCESSING OF THICK TANTALUM SILICIDE FILMS

5.1 Stress in Thick Tantalum Silicide Films

The first two problems that presented themselves in using tantalum silicide as the primary electromechanical material for the micromotors stemmed from the fact that the tantalum silicide needed to be deposited at thicknesses in excess of 1μm. Initial depositions of tantalum silicide were greater than 3μm, and the quality of the as-deposited films was exceptional (very high reflectivity, and a grainsize too small to be seen at 1000X). There were no signs of stress, and there was no evidence of graininess, as there typically is in LPCVD polysilicon. The first problem was that the thick tantalum silicide films were subject to stress-related cracks and peeling during any high temperature processes that followed deposition. The second was that anisotropic etching of the thick films was difficult with the equipment available at that time at NJIT's MRC. The second problem will be discussed in section 5.2.

As mentioned in chapter 4, deposition of tantalum silicide is typically followed by a high temperature sintering process. This is primarily to reduce the electrical resistivity of the material [17]. Since the electrical properties of tantalum silicide were not of primary concern for the micromotors, it was decided that sintering was not necessary. In order to be sure that the mechanical integrity of tantalum silicide would not be sacrificed, a simple test was performed. Tantalum silicide (approximately 1μm thick) was deposited on approximately 9000Å of SiO_2. Cantilever beams (5μm wide, 5μm separation) were patterned in the tantalum silicide, and released in 7:1 BOE. The beams showed no signs of warpage, and were remarkable strong (a beam 100μm long was bent 90°, and sprang

back to its original shape with no sign of damage). This demonstrated that sintering of the tantalum silicide was not necessary to ensure the mechanical integrity of the material. However, since subsequent processing steps required that the film be exposed to temperatures up to 380°C, it was necessary to confirm tantalum silicide's ability to withstand such temperatures.

At first, sintering of the tantalum silicide films was done at 500°C. Since the temperature of the subsequent LTO deposition that was to be used was 380°C, 500°C provided plenty of processing latitude.

The test samples were approximately 9500Å of steam oxide, with approximately 2μm of tantalum silicide sputtered over it. Both patterned and unpatterned wafers were annealed. The anneal was done for 30 minutes at 500°C, under nitrogen. As the unpatterned wafer was removed from the furnace tube, it appeared to be unaffected by the anneal. However, as the wafer cooled, cracks began to develop on the wafer. The macroscopically visible cracks were oriented at approximately 45° angles to the primary flat of the wafer (<100> orientation). Similar results were observed for sintering temperatures of 900°C, as well as 400°C. Annealing times were also varied, from 30 minutes up to 2 hours, again with no change in the cracking of the films.

The patterned wafers used for the annealing experiments also showed significant cracking and peeling. However, they showed something that was not seen on the unpatterned wafers. By looking at an annealed patterned sample with a SEM, it was apparent that the tantalum silicide was not peeling from the oxide as was originally thought; rather, the tantalum silicide to oxide adhesion was quite good, as was the oxide to silicon adhesion. The stress induced in the tantalum silicide was actually causing concordial fractures of the silicon substrate, lifting large pieces of silicon up with the tantalum silicide and the oxide. Figure 5.1 shows a scanning electron micrograph of this phenomenon. Along the pad to stator interconnect, most of the substrate is very bright, except for a small portion of it near the pad, which is darker. The area where the pad used

to be is also dark. The bright area is where the oxide remained attached to the substrate (since it is an insulator, it absorbs and holds charge, thus appearing brighter in the SEM). The darker areas are where the oxide was lifted off with the tantalum silicide. By using a step profiler, the depth of the cavity where the tantalum silicide pad used to be was measured. Including the thickness of the oxide, the cavity was nearly 6μm deep. This means that approximately 5μm of silicon was torn from the rest of the substrate by the tantalum silicide pad. This indicates the incredible strength of the tantalum silicide to oxide bond, as well as the enormous amount of stress in the film after annealing. An optical micrograph of the cavities formed is shown in Figure 5.2.

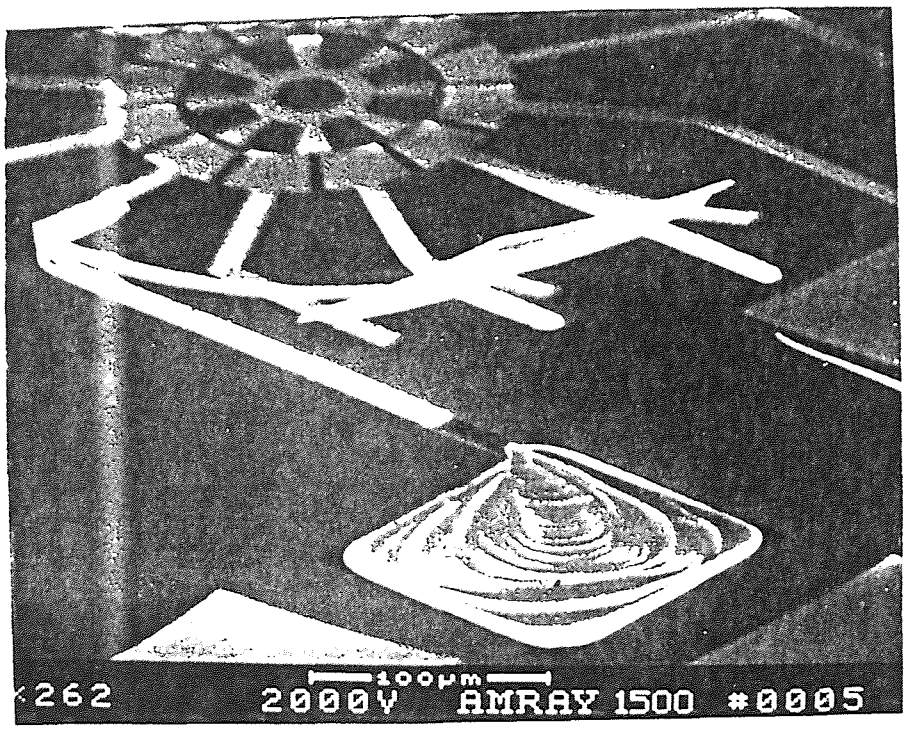

Figure 5.1 Scanning electron micrograph following the annealing of 1.5μm tantalum silicide at 900°C. Notice the very bright areas, which indicate the presence of SiO_2 still remaining on the substrate, except at the location where the pad used to be.

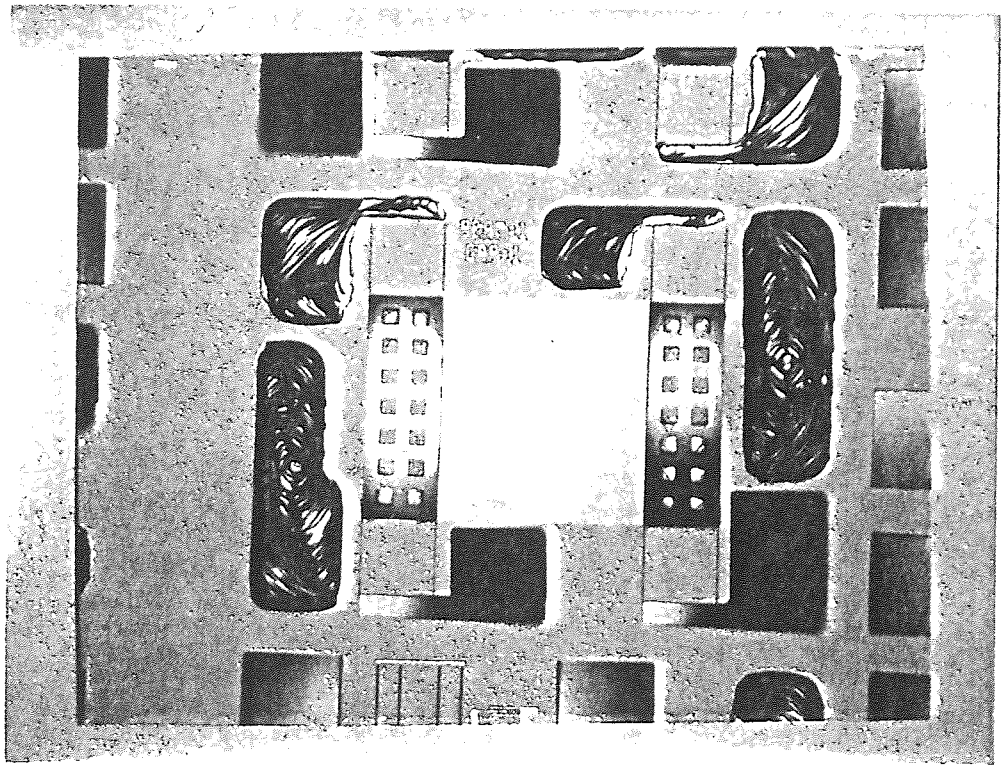

Figure 5.2 Optical micrograph showing the cavity left where a bonding pad peeled from the substrate after annealing (1.5μm tantalum silicide).

In some areas, peeling of the tantalum silicide features did not occur; rather, the film merely cracked. Figures 5.3 and 5.4 are optical micrographs showing two different areas of a wafer. Figure 5.3 shows cracks that occurred on the bonding pads of a test structure on the mask set. The pads around the one in the center all exhibited the peeling and substrate fracturing discussed previously. Figure 5.4 shows a close-up of the micro-cracks seen on an unpatterned, annealed sample of tantalum silicide.

Since the issue of tantalum silicide's ability to withstand the 380°C LTO deposition was still not resolved, further experimentation was necessary. Thinner films of tantalum silicide were deposited and annealed at 900°C (this was the temperature at which the least

amount of damage was seen in the thicker films). Three wafers were used for this experiment, with film thicknesses of 7500Å, 1μm, and 1.25μm. After annealing at 900°C, all three wafers looked good. Within the first hour, a few micro cracks developed on the wafers with 1μm and 1.25μm of tantalum silicide. The 7500Å sample still looked good. Approximately 18 hours later, all but the 7500Å sample had peeled as before.

Further processing was performed on the 7500Å sample, in order to simulate that to which the device wafers would be subjected. The wafer was patterned, then annealed at 400°C for one hour to simulate an LTO deposition. The wafer still looked good. The one concern was that the film would not be thick enough for the motors to work well;

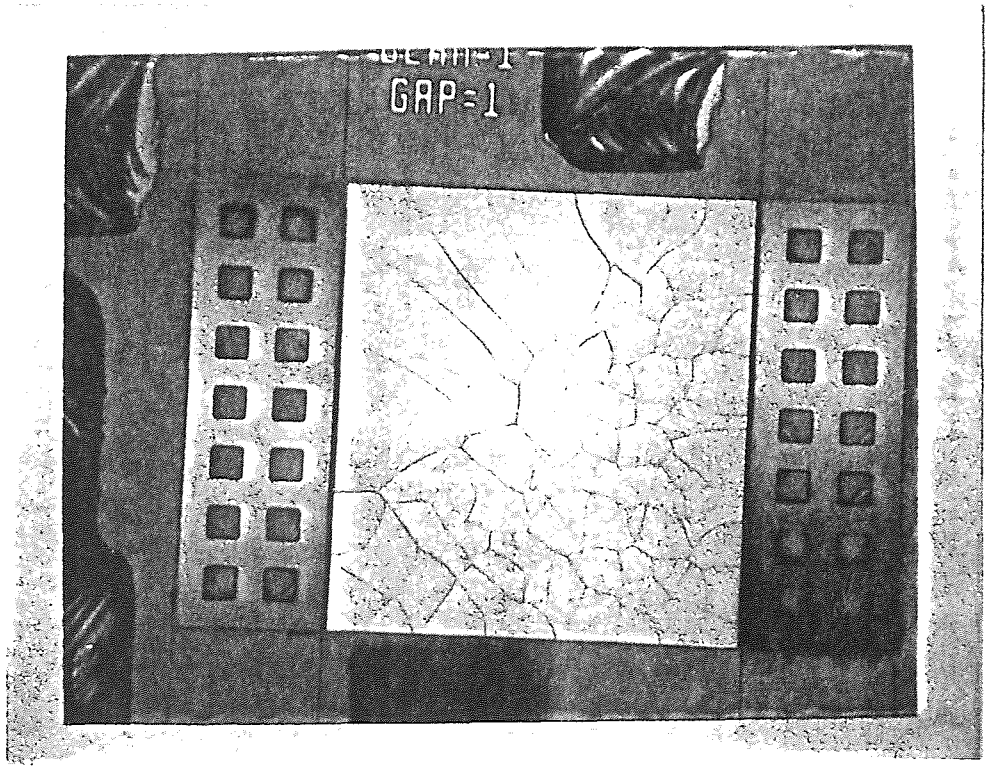

Figure 5.3 Optical micrograph of a cracked bonding pad after annealing at 350°C (tantalum silicide thickness: 1.5μm).

however, 7500Å was worth a try. When 7500Å of tantalum silicide was deposited on one of the device wafers, however, different results were obtained. After the anneal, some peeling was visible around the edge of the wafer. When inspected under a microscope, it was seen that in areas where the tantalum silicide had covered a step, the film had cracked. Twenty-four hours later, the peeling and cracking was even worse. This meant that even a film as thin as 7500Å of tantalum silicide was not going to withstand high temperatures.

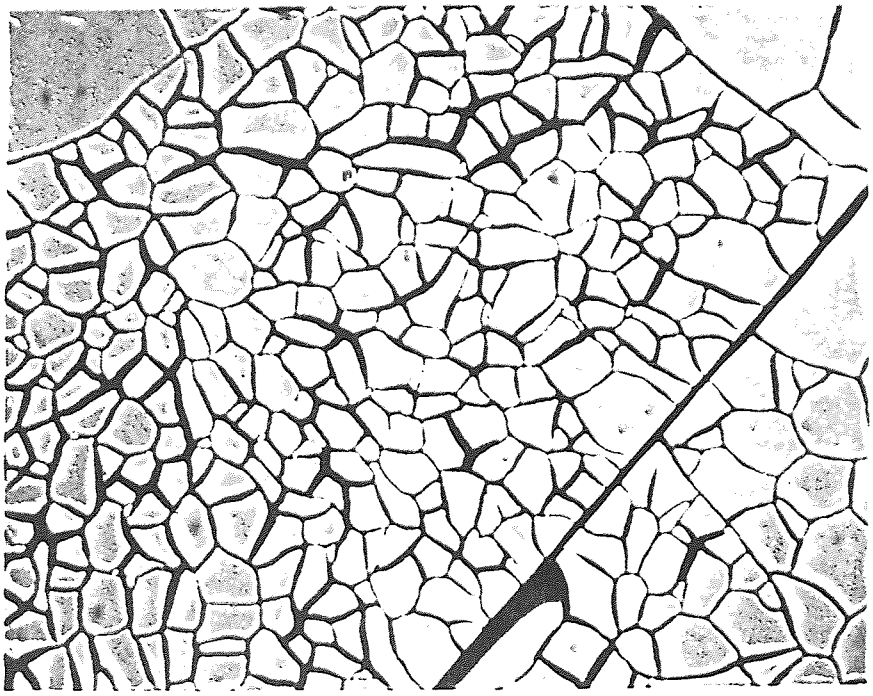

Figure 5.4 Optical micrograph at 100X showing micro-cracks on an unpatterned, annealed tantalum silicide film (1.5μm thick).

At this point, an alternative for the 380°C LTO was sought. A PECVD LTO process with a deposition temperature of 300°C was made available to NJIT. Since this would be the highest temperature the tantalum silicide would need to see after deposition, tests were run to ensure that 300°C would not be a problem. In fact, it was not. No cracking or peeling occurred for films annealed at 300°C, either patterned or unpatterned. Films annealed at 325°C, however, did exhibit stress-related failure.

Investigation into this revealed that at approximately 300° to 350°C, tantalum silicide makes a transition from compressive to tensile stress (this occurs when the as-deposited tantalum silicide begins to densify) [17]. At approximately 400°C, the film begins to crystallize, and the stress continues to increase until the temperature reaches approximately 450° to 500°C, above which temperatures the stress in the film remains relatively constant [18]. Figure 5.5 shows a plot of stress vs. temperature during the sintering of a 2300Å tantalum silicide film.

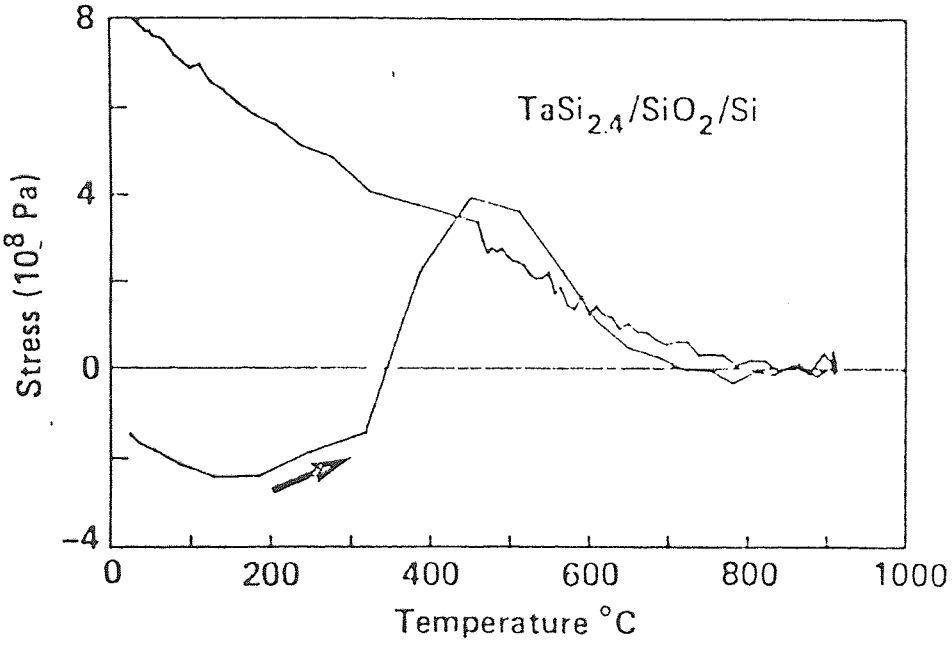

Figure 5.5 Stress vs. temperature for a 2300Å tantalum silicide film during sintering on an oxidized silicon wafer. Arrow indicates direction of heat treatment cycle [17].

Based on the results of the many sintering experiments, and also on the fact that a 300°C LTO process was made available, it was decided to use a thick (>1μm) tantalum silicide film, and to limit the temperature to which the film was exposed after deposition.

5.2 Plasma Etching Thick Tantalum Silicide Films

The final thickness of the tantalum silicide used for the micromotors was ultimately determined by its ability to be etched anisotropically in the plasma etcher available at that time at NJIT's MRC. Films in excess of approximately 2μm required such long etch times that the photoresist thickness necessary to last through the etch effectively prevented defining the 1μm rotor/stator gap. In addition, since so much photoresist degradation occurred in the long plasma etches, gaps that initially were 1μm were increased to more than 2.5μm in the etched film. This section summarizes the approximately 50 experimental etches performed on thick tantalum silicide films.

Initial etches were done based on Drytek recommended etch recipes using a Drytek DRIE-100 plasma etcher. The starting parameters were as follows: 25sccm SF_6, 25sccm Freon 115, 500 Watts, 200mTorr, 25°C. This etch worked well for a thin film (less than 1μm), with an etch rate of approximately 750Å/minute. When a thicker film was etched using this recipe, severe undercutting of the photoresist was seen. Figure 5.6 shows an optical micrograph of one of the initial etches. The bright areas are the remaining tantalum silicide, visible through the photoresist. The darker area surrounding the tantalum silicide is the photoresist. The amount of undercutting is approximately 5μm (the width of the stator interconnects is 12μm).

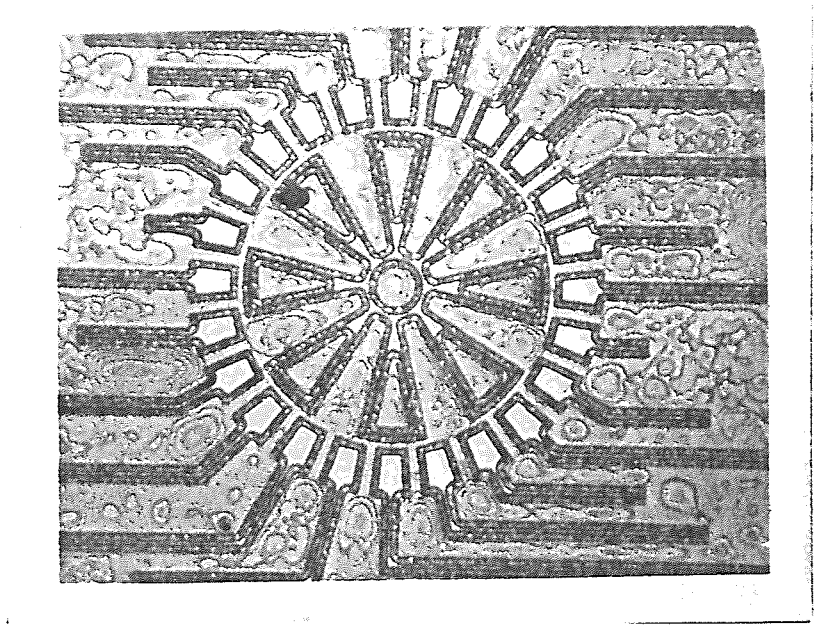

Figure 5.6 Optical micrograph showing the substantial and unacceptable undercutting of photoresist in one of the initial tantalum silicide etches. The photoresist has not been removed.

Reactive ion etching of tantalum silicide has been studied in a CF_4/O_2 plasma [19]. Although the etcher used at NJIT was a plasma etcher, not a reactive ion etcher, it was hoped that the systems would be similar enough that the chemistries would perform similarly. A CF_4/O_2 plasma resulted in relatively sharp sidewalls, with only a small amount of undercutting. However, the etch rate of the tantalum silicide was only about 200Å/minute, with a selectivity to photoresist of approximately 0.83:1. This was not acceptable. By eliminating the oxygen in the etch, the selectivity to photoresist was increased to approximately 2.70:1. The etch rate increased to about 540Å/minute, but the quality of the etch decreased. After etching 5400Å of tantalum silicide, a brownish, speckled 'residue' was apparent on the surrounding substrate. The degree of anisotropy

was about the same. By using SF_6 in place of CF_4 (to provide more available free fluorine - the primary etchant here), the etch rate was dramatically increased to approximately 2200Å/minute. However, the etch was completely isotropic, and the substrate turned brown, similar to the CF_4 etch.

Since the silicide etch recipe recommended by Drytek is identical to that for silicon/polysilicon, the same parameter dependence was assumed; namely, that SF_6 alone would provide a high etch rate, but with significant undercutting, while Freon 115 alone would give a vertical sidewall, but with low etch rates. Based on this, Freon 115 alone was tried as an etchant gas. A short etch showed that the etch rate of tantalum silicide was approximately 400Å/minute, with a selectivity to photoresist of approximately 5.1:1. The etch showed no undercutting, and a very slight brownish color of the surrounding substrate. A longer etch did not provide such positive data, however. After a 65 minute etch, the entire wafer looked black under a microscope. This was thought to be a severe case of the brownish speckling problem discussed previously.

An explanation of the speckling was hypothesized as follows: the speckling seen after etching tantalum silicide resembles that seen when etching a film of aluminum/silicon in a phosphoric/nitric/acetic/water mixture. The solution etches the aluminum, but does not etch the silicon contained in the film. The result is a reddish-brown speckling of the substrate after the aluminum has been removed. The speckles are the small amount of silicon that was not dissolved during the etch. The same may be true for tantalum silicide. The silicon probably etches much faster than the tantalum, and therefore the tantalum would be 'precipitated out' during the etch, leaving the brownish residue seen. Figure 5.7 shows a linewidth feature with a dark haze around it. This is an example of what was seen on the etched substrates.

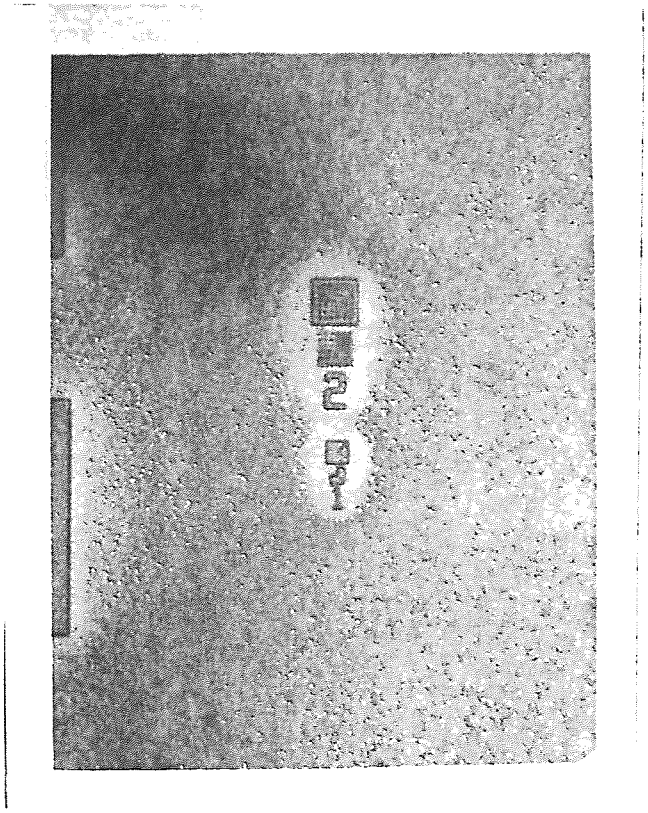

Figure 5.7 Optical micrograph showing speckling of substrate around the plasma-etched features in tantalum silicide (1μm and 2μm linewidth features shown).

Several more etch experiments with tantalum silicide were performed, including two Designs of Experiment [24]. Several of the etches seemed to be reasonable in all respects except in selectivity to photoresist. To help circumvent the problem of photoresist loss during the long etches necessary for the thick films used here, an aluminum masking layer was used to supplement the photoresist. Figure 5.8 shows the result of an etch performed using a thin layer (1000Å) of aluminum as a mask. The aluminum either did not hold up to the etch, or did not adhere well to the tantalum silicide. Apparently, it did last at least part way through the etch; the abrupt step from the edge of the remaining aluminum to the underlying tantalum silicide shows that there was some undercutting before the aluminum failed. Thicker aluminum films (up to 4000Å) were tried, but were never used for the micromotor fabrication.

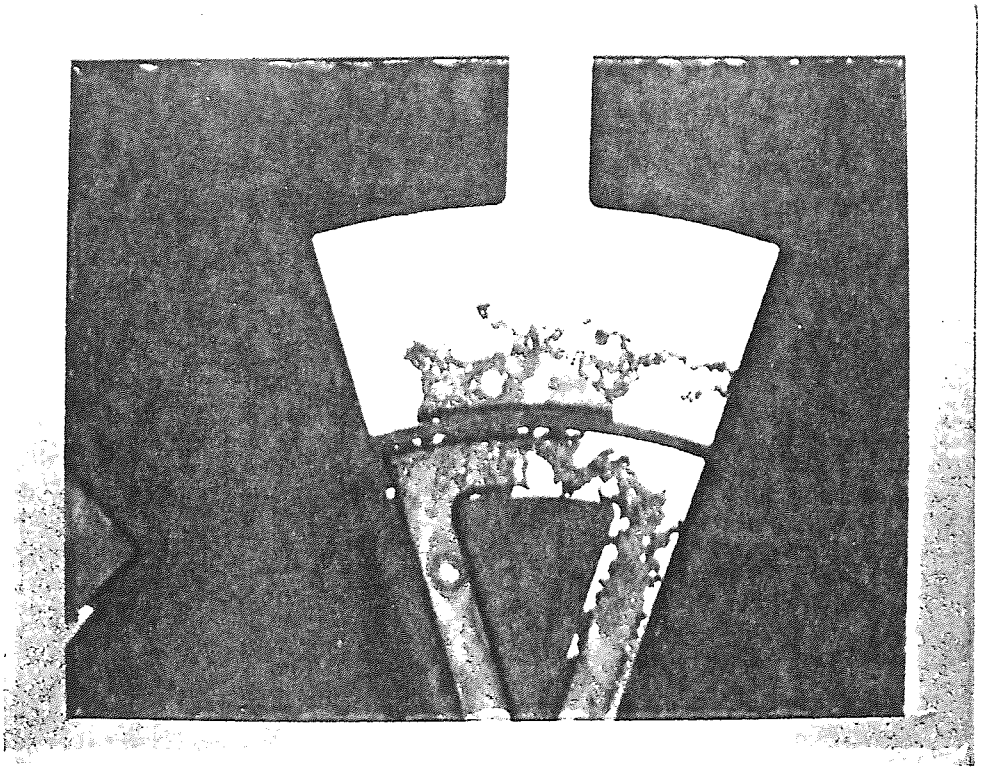

Figure 5.8 Aluminum mask degradation after a tantalum silicide plasma etch (1000Å Aluminum on 2.5μm tantalum silicide).

The tantalum silicide etch finally decided upon is given in chapter 4. It was based on a combination of previous works [20, 21], and upon the extensive experimentation performed at NJIT. The aluminum mask was not needed for the etch and film thickness combination ultimately used; the added complexity of its use was not compensated by a significant improvement in etch quality over simply using photoresist. Figure 5.9 shows a 150μm diameter rotor patterned in 1.5μm tantalum silicide, using photoresist as the etch mask, and the etch recipe given in chapter 4. The nominal rotor/stator gap was 1μm; the actual gap was slightly over 2μm.

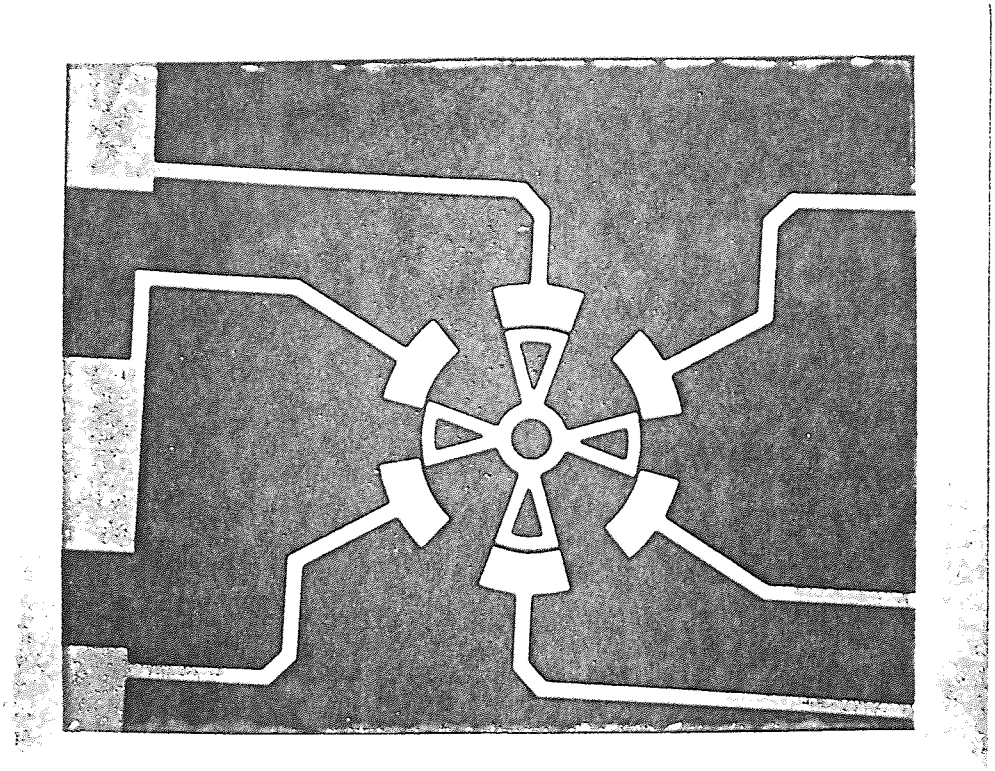

Figure 5.9 A 150μm diameter rotor plasma etched in 1.5μm of tantalum silicide with a rotor/stator gap of slightly over 2μm.

5.3 Wet Etching of Tantalum Silicide

Wet etching of tantalum silicide is possible in at least two types of solutions. The first is a silicon etching solution of nitric acid (HNO_3), HF, and acetic acid (CH_3COOH). The second is in hydrofluoric acid alone. As discussed in Chapter 4, the fact that tantalum silicide seems to be so highly soluble in HF made successful release of the completed micromotors impossible in this work. The details of the problems encountered will be discussed.

Using a solution of 40 parts (by volume) HNO_3, 1 part (by volume) HF, 2 parts (by volume) CH_3COOH, and 20 parts (by volume) H_2O, tantalum silicide films can be isotropically etched. The etch rate of tantalum silicide in the solution at room temperature

(approximately 23°C) is approximately 1000Å/minute. The etch rate of SiO_2 is also very near 1000Å/minute, and the etch rate of silicon is even higher. Therefore, this etch must be used very cautiously in etching tantalum silicide films, or in stripping wafers of tantalum silicide. Damage to the underlying substrate can be done very easily.

The etch rate of tantalum silicide in various HF solutions is still not clear. Consistent results have been difficult to obtain. Before work on the tantalum silicide micromotors began, the etch rate of tantalum silicide in 49% HF was measured in order to be sure that the completed devices could be successfully released. These initial experiments showed that the etch rate of tantalum silicide in room temperature 49% HF was approximately 400Å/minute. Since a minimum of 5 minutes in the HF would be necessary for release of the devices, approximately 2000Å of tantalum silicide from each side of the rotor would be consumed during the release; a total of 4000Å would be lost. If the rotor was thick enough, though, this shouldn't have been a problem.

As was previously discussed, significantly more than 4000Å of tantalum silicide was lost in the release etch. A five minute release in 49% HF consumed all of the 1μm tantalum silicide bearing, and significantly damaged the rotor/stator level (see Figure 5.10). A step profile of the remaining tantalum silicide at the bonding pad locations indicated that approximately 7000Å of tantalum silicide was lost during the 5 minute release etch. This corresponds to an etch rate of 1400Å/minute, over 3 times faster than initially measured.

Using 7:1 BOE at room temperature as the release agent was no more successful. Figure 5.11 shows the result of an 80 minute release etch in BOE. Only one of the six stators remains intact, and the center bearing is gone. As was the case with 49% HF, however, the rotor is still not free (otherwise it would have floated away in the etch). Step profiler measurements indicated that only about 4500Å of tantalum silicide was consumed at the bonding pad locations, yet the center bearing (initially 1μm thick) was completely gone. Diluting the BOE 1:1 with glycerin (a mixture similar to that used to

protect aluminum from BOE during contact window etches in CMOS circuits) served only to slow down the etch rate of the oxide as well as that of the tantalum silicide.

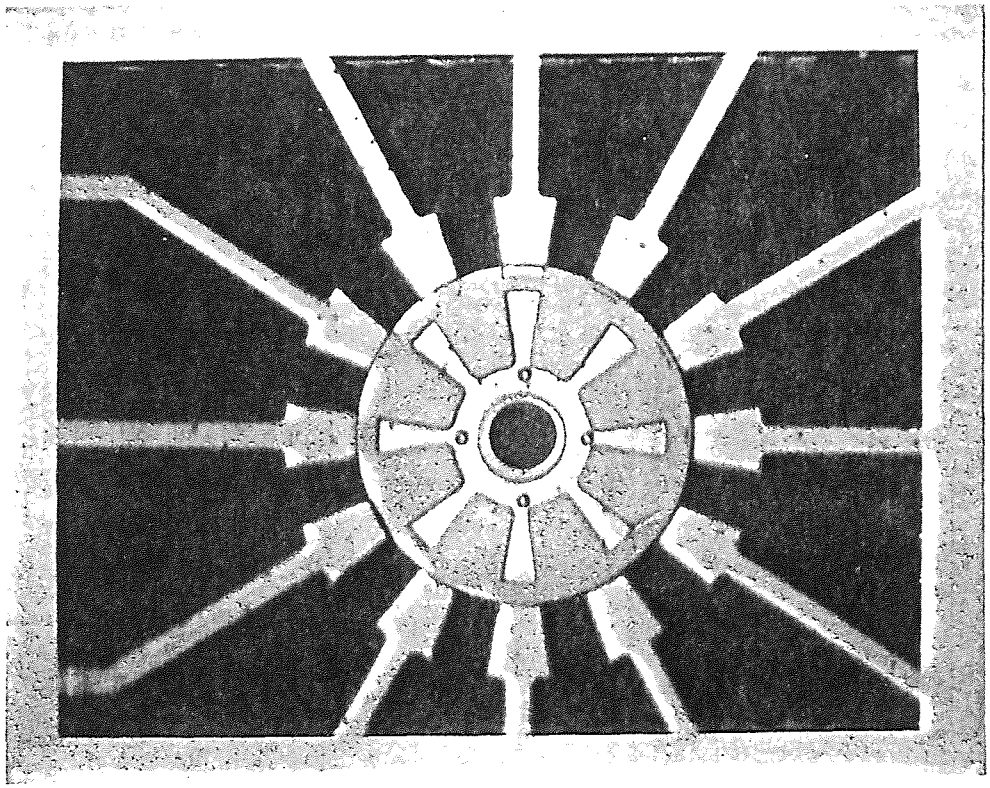

Figure 5.10 100μm diameter motor released 5 minutes in 49% HF. Notice the pieces of the stators that broke off during the release, and the absence of the center bearing.

Following these unsuccessful release attempts, the etch rate of tantalum silicide was again measured on an unpatterned wafer. The tantalum silicide was deposited on a bare silicon wafer which was partially masked. The height of the step remaining on the wafer was measured using a step profiler. The tantalum silicide was then etched for 2 minutes in 49% HF at room temperature. The height of the step was measured in the same place as before. The difference in the step measurements was approximately 1000Å, which is an etch rate of 500Å/minute. This number corresponds closely to the initial

measurement of the etch rate, and in no way predicts the results seen on the micromotor device wafer.

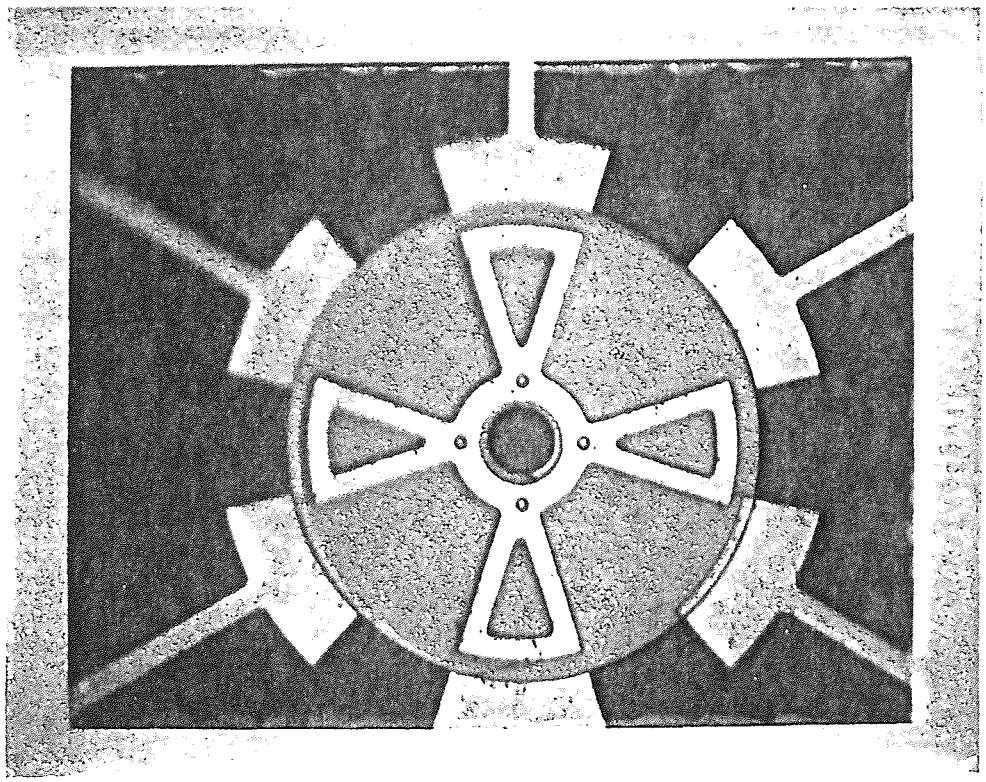

Figure 5.11 150μm diameter motor released 80 minutes in 7:1 BOE at room temperature.

One explanation is that the tantalum silicide is not being etched by the HF solutions, but rather is being lifted off the substrate by them. This seems to be a possible explanation for the complete disappearance of the 1μm thick center bearing during a 5 minute release etch. Further study of the tantalum silicide/silicon nitride interface is needed to understand this phenomenon.

CHAPTER 6

APPLICATION: PROGRAMMABLE NON-VOLATILE VARIABLE CAPACITOR

6.1 Introduction

A novel application of the technology employed in the variable capacitance rotary micromotor is a programmable non-volatile variable capacitor. As the name implies, this is a device which can be electrically programmed to a specific value of capacitance, and which will remain at that capacitance without the need for a continuous power supply. The varying capacitance is obtained mechanically, by positioning a movable semicircular plate (analogous to the rotor of the rotary micromotors) with respect to a fixed semicircular plate, with side-drive electrostatic actuation. Figure 6.1 shows a simplified top view of the proposed device.

By applying a series of pulses to the stators to rotate the upper electrode counter-clockwise, the rotor can be reset, or brought to rest against the stop shown at the top of the rotor in Figure 6.1. By then applying a specific number of pulses to the stators, the angularly positionable top electrode can be rotated clockwise in increments related to the number of stator and rotor poles. Since the rotor is a semicircle, the capacitance between it and the fixed semicircular electrode on the substrate varies with rotor position. By accurately controlling the positioning of the rotor, the capacitance of the device can be programmed precisely. Electrical contact to the upper electrode is achieved through support pins on the upper electrode (similar to the support pins on the rotor of the micromotor) which ride on a contact ring on the substrate, and also through the center bearing.

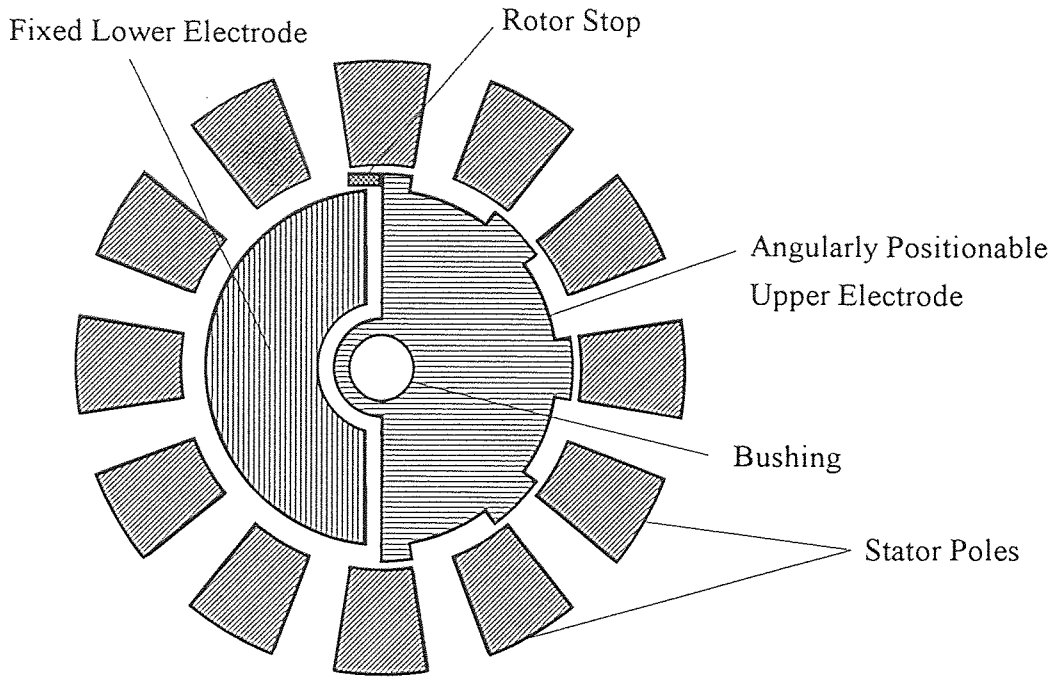

Figure 6.1 Simplified plan view of the programmable non-volatile variable capacitor. Note rotor stop (cross-hatched rectangle).

Applications of this microelectromechanical device include replacement of voltage variable capacitors (varactors or varicaps), and replacement of manually adjustable trimmer capacitors. This device has the advantage of minimal shunt losses as compared with forward biased varactors. Programmable variable capacitors can also be fabricated on the same substrate as microelectronic circuits.

6.2 Theory of Operation

In order to understand the operation of the programmable variable capacitor, a simple model of the parallel plate capacitor can be used. Figure 6.2a shows a cross section of the

programmable variable capacitor through the center of the device, with the upper and lower electrodes positioned as fabricated (not aligned with each other). Figure 6.2b shows the same cross section with the upper electrode rotated so that it is aligned with the lower electrode, and with the sacrificial layers removed. From these two views, the size of the gap between the upper and lower electrodes can be easily understood. The gap is equal to the thickness of the Oxide1 layer, less the thickness of the lower electrode (Metal1), and less the distance from the bottom of the upper electrode support pin to the top of the upper electrode contact ring. Assuming an Oxide1 thickness of 1.0μm, a Metal1 thickness of 5000Å, and a 1000Å distance between the bottom of the support pin to the top of the upper electrode contact ring, the gap between the upper and lower electrodes would be 4000Å.

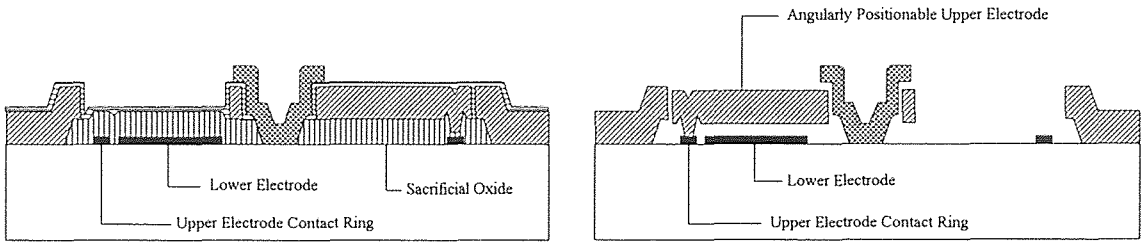

(a) (b)

Figure 6.2 Cross sectional views of the programmable variable capacitor, showing (a) the non-aligned upper and lower electrodes, unreleased, and (b) the aligned upper and lower electrodes following sacrificial oxide removal.

The other important parameter in determining the maximum capacitance of the device is the area of overlap of the upper and lower electrodes. By examining Figure 6.1, it can be seen that the maximum overlap area is equal to the area of the lower electrode. Assuming that the lower electrode is a semicircle with outside radius 200μm, and with an

inner semicircular cutout of radius 20μm, the area of the lower electrode is approximately 62,000μm^2. Using a parallel plate approximation which neglects fringing fields, the maximum capacitance of such a device is approximately 1.4pF, with air as the dielectric between the plates of the capacitor. Figure 6.3 shows a graph of maximum capacitance vs. rotor radius for values of radius up to 10mm, and for gap spacings of 0.4 and 0.8μm. By using a high dielectric constant liquid between the plates, the capacitance of the device could be increased. Without simulations of the fringing fields in the device, it is impossible to determine the minimum capacitance of the device when the upper and lower electrodes are maximally misaligned (as shown in Figure 6.1).

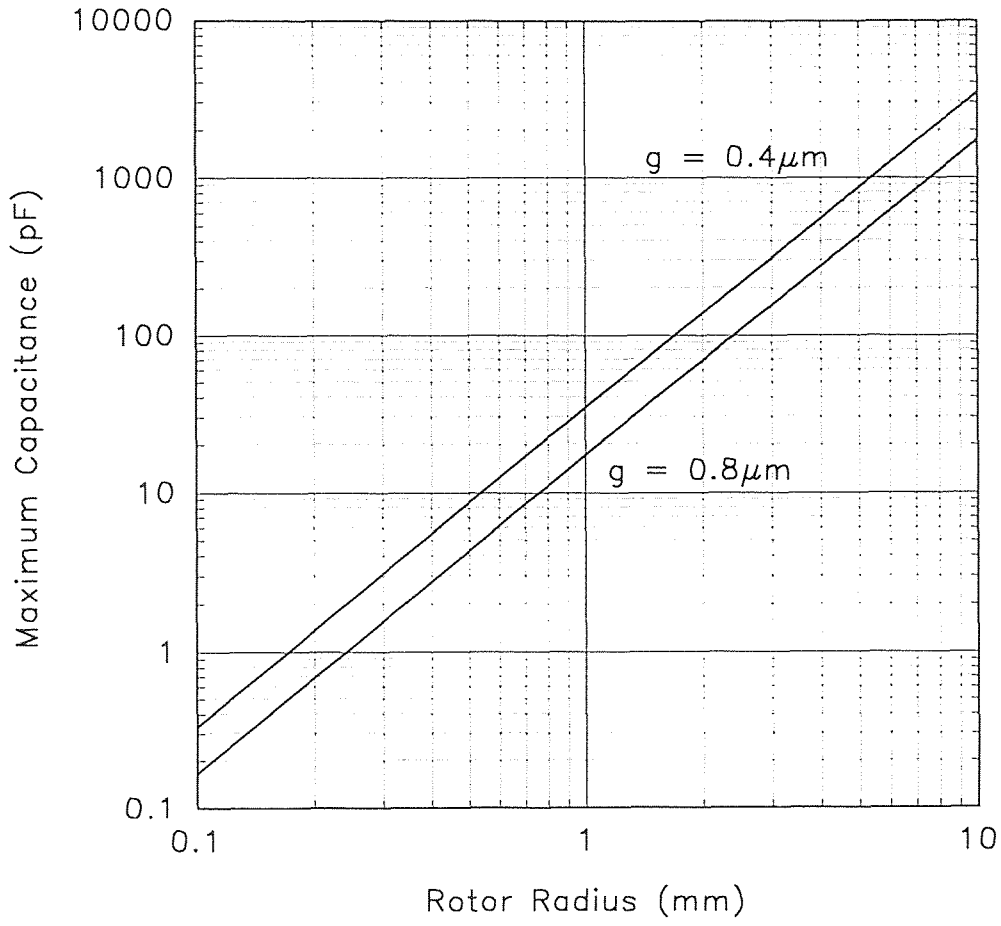

Figure 6.3 Maximum capacitance vs. rotor radius for rotor radius values up to 10mm, and gap spacings of 0.4μm and 0.8μm (parallel plate approximation).

To position the upper electrode, the same principles are used as are used to drive the rotary micromotors. Since the motors are driven by a stepped DC signal, they operate as stepper motors. Each pulse rotates the motor by 15° (for the 12:8 geometry). If the programmable variable capacitor were fabricated to correspond to a 12:8 motor geometry, the same would hold true. This would mean a total of 12 values of capacitance that could be programmed. With the 3:2 stator:rotor pole ratio, the number of programmable capacitance values is equal to the number of stator poles. A more finely programmable device could be designed by varying the ratio of stator to rotor poles, as well as by simply increasing the number of stator poles.

The programming is accomplished by means of a stepped DC signal, just as with the micromotors. First, the upper electrode would be driven counterclockwise with a series of pulses long enough to bring the electrode to rest against the stop (see Figure 6.1). This ensures that the upper electrode is always starting from the reset position. To program the capacitor, a series of pulses is applied to the stators to rotate the upper electrode to the desired position. By controlling the number of pulses applied, the final position of the upper electrode can be controlled. For example, in order to rotate the upper electrode of a 12:8 device 90° from the reset position, 6 pulses need to be applied (15° per pulse). The capacitance of the device would then be set at the value calculated for a 90° overlap of the upper and lower electrodes.

6.3 Fabrication

The fabrication sequence for the programmable variable capacitor is very much like that for the rotary micromotors. The main difference in fabricating the programmable variable capacitor is that it requires a lower metal layer in which the lower electrode and the contact ring are patterned. Figure 6.4 shows the detail of the contact ring and upper

electrode support pins, as well as the necessary connections to the contact ring and lower electrode. Note that a contact for the bushing is shown in this figure. This would help to ensure a good contact to the upper electrode. Also, the capacitor must be fabricated on an insulating substrate, or with an insulating layer on a silicon substrate. Figure 6.5 shows the process flow for the programmable variable capacitor.

The materials of construction must be chosen very carefully for this device. The upper and lower electrodes must be conductive, and the contact between the upper electrode and the contact ring must be very low resistance, since it is desirable to have as high a device Q (low series resistance) as possible. There are two specific requirements for the materials to ensure an ohmic contact between the upper electrode and the contact ring while maintaining the necessary mobility of the upper electrode. The first addresses the issue that good electrical contact must be maintained between the upper electrode and contact ring. Since the nature of the device is that it could be static for extended periods of time, it is necessary that the materials used for the electrodes be such that any native oxide formation be minimized, or even eliminated. Secondly, it is necessary that after such extended static periods the upper electrode still be free to move if the capacitance of the device is to be varied.

The first requirement suggests that silicon (single crystal or polycrystalline) is not a suitable material, since the native oxide formation would eventually increase the contact resistance and lower the device Q to an unacceptable level. In order to avoid excessive stiction of the upper electrode to the contact ring, it is desirable to use dissimilar metals for the upper electrode and contact ring. Similar metals are subject to molecular interaction, and possibly such phenomena as fusion bonding. By using dissimilar materials, molecular interactions are minimized. Two possible metallurgies include palladium and platinum, or palladium and gold.

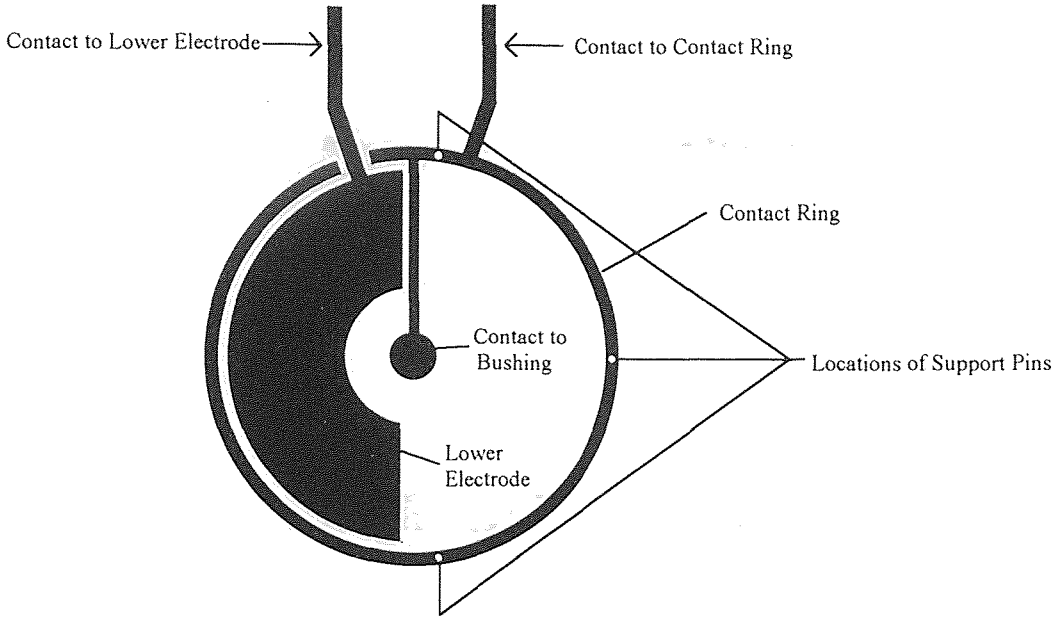

Figure 6.4 Detail of contact ring, upper electrode support pin locations, and lower electrode contact (upper electrode omitted for clarity).

6.4 Conclusion

The programmable non-volatile variable capacitor has great potential applications as a discrete surface mount device in microwave integrated circuits. Presently the only non-volatile variable capacitor available for such applications is a mechanically adjustable trimmer capacitor. These devices are typically surface mount devices that employ Tape Automated Bonding (TAB) techniques for mounting to a substrate. The maximum to minimum capacitance ratio for such devices has a maximum value of approximately 7, but is more typically approximately 4 [22].

facing 65

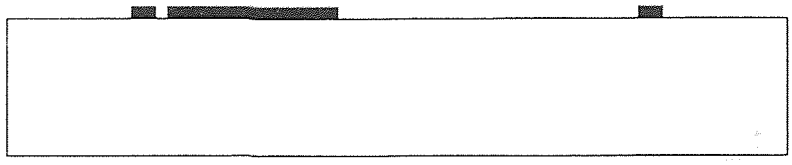

(a)

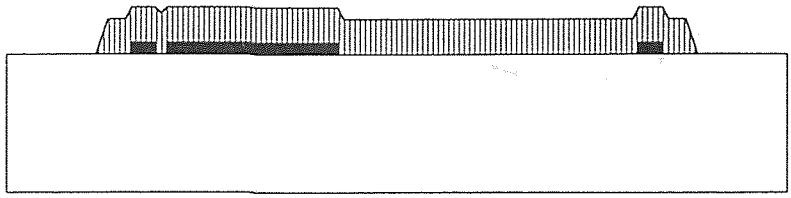

(b)

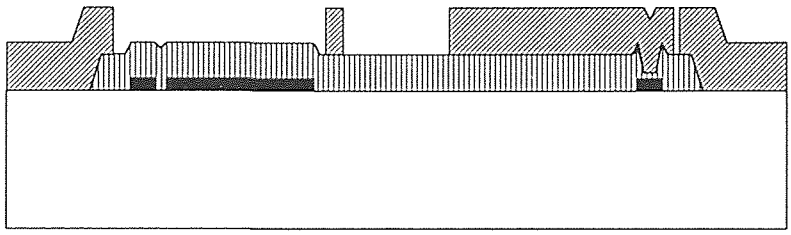

(c)

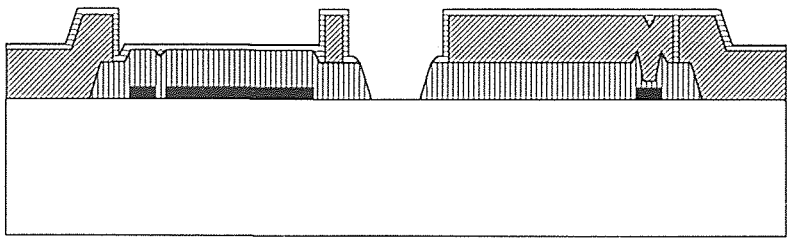

(d)

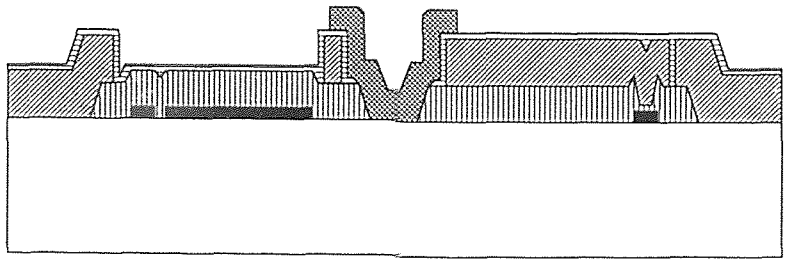

(e)

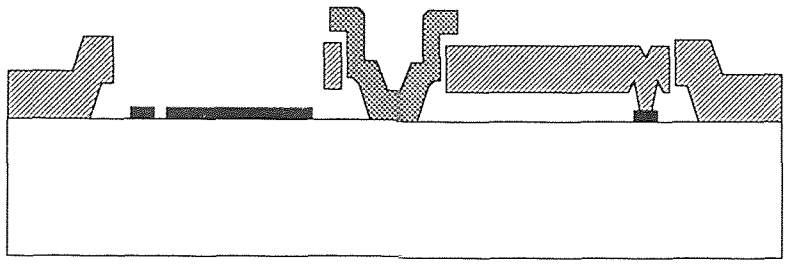

(f)

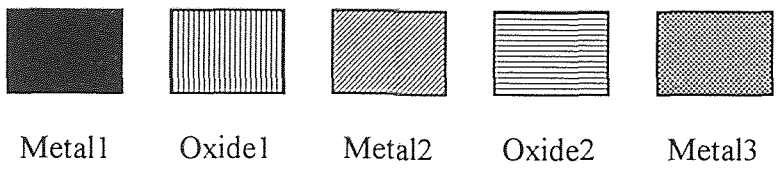

Figure 6.5 Process flow for the programmable variable capacitor fabricated on an insulating substrate; (a) patterned Metal1 layer for lower electrode and contact ring, (b) patterned Oxide1 sacrificial layer, (c) patterned Metal2 for upper electrode and stators, (d) Oxide2 with bushing anchor etched through it and Oxide1, (e) patterned Metal3 bushing, and (f) complete released device.

CHAPTER 7

SUMMARY AND CONCLUSIONS

7.1 Tantalum Silicide as a Microelectromechanical Material

Tantalum silicide was chosen to be used as the primary microelectromechanical material for the variable capacitance rotary micromotor based on its low resistivity, compatibility with standard silicon processing techniques, and high temperature capability, but mainly due to its lack of surface roughness compared to typical LPCVD polysilicon films.

Tantalum silicide, as available in NJIT's MRC, exhibits extreme tensile stress when annealed, and appears to be incompatible with HF solutions after patterning. It is still unclear exactly what mechanism is responsible for the problems encountered during the release etch; whether the tantalum silicide is soluble in HF solutions and is therefore dissolving, or whether the interface between tantalum silicide and silicon nitride is not stable when exposed to HF solutions, and is therefore inducing lift-off of the tantalum silicide. In either case, the fact that the tantalum silicide layers are severely damaged or even completely destroyed during the release etch means that additional work needs to be done to understand these mechanisms more fully.

A novel application of the rotary micromotor, the programmable non-volatile variable capacitor, was introduced, and the processing of the device discussed. The programmable variable capacitor could be used in surface mount applications in microwave circuits, replacing the mechanically adjustable trimmer capacitors currently in use.

7.2 Suggestions for Future Work

If tantalum silicide is to be pursued as a microelectromechanical material, it is necessary that the release etch selectivity of oxide to tantalum silicide be increased. This can be done in two ways: either increase the etch rate of the oxide, or decrease the etch rate of the tantalum silicide.

In order to increase the etch rate of the silicon dioxide sacrificial layer, two options are readily apparent. The first would be to grow a phosphorous-doped oxide during the LOCOS process, thereby increasing the etch rate. This unfortunately was not possible in NJIT's lab. This option still allows the use of the LOCOS process for fabrication simplification.

The other option is to change the fabrication process from the LOCOS process to the 'standard' process, where instead of using a thermally grown oxide as the sacrificial layer, a deposited low temperature oxide is used. This means that the topography on the substrate becomes very large at the end of the process. However, since the etch rate of deposited low-temperature oxides can be as high as 5 to 10 times that of thermal oxides, the larger topography may be an acceptable alternative.

A third but much more difficult to implement option is to follow the process sequence of the LOCOS process, except that instead of thermally oxidizing the silicon, use a spin-on glass (SOG) as the sacrificial layer. Again, the etch rate of SOG can be significantly higher than that of thermal oxides. The problem with SOG is that the maximum thickness for a single coating is typically less than 1μm, and that the SOG tends to planarize (very much like photoresist; sharp corners will be rounded off, but different levels of topography will still be present). By using several layers of SOG spun on sequentially, the thickness could be increased to the desired value, and the planarity of the substrate could be maintained by subsequently etching back the SOG, possibly requiring an additional mask level.

Decreasing the etch rate of the tantalum silicide rotor and stators is the other option available to help preserve the integrity of the micromotors. It is possible that this could be done by varying the chemistry of the etch used for the sacrificial oxide removal. This approach would be best left to a chemist.

Another option is to use a different material in which to encase the tantalum silicide components. A thin layer of polysilicon, for instance, could be used to cover the top and bottom of the rotor and stators, thus protecting them from the HF solution. As long as the polysilicon is relatively thin (less than approximately 1000Å), the surface roughness of the polysilicon is not significant. However, due to the upper temperature limit of 300°C for thick tantalum silicide films, it would be necessary to deposit the polysilicon by a low temperature process, such as sputtering or PECVD.

Similarly, use of a thin layer of silicon nitride or silicon carbide would achieve the same effect (the temperature must still be monitored carefully during the deposition of any encapsulant). Also, a thin layer of an HF insoluble metal such as platinum would serve to protect the tantalum silicide, while still maintaining the benefit of the smooth surface of tantalum silicide.

The options presented to help preserve the integrity of the tantalum silicide during the release of the motors in general would require additional masks, or in some cases, a different mask set. One exception is the option of growing a phosphorous doped oxide during the LOCOS process. The other possible exception would be the case where the tantalum silicide is encased in another material. Without very careful consideration of the processing techniques needed to successfully achieve this, it is difficult to predict whether additional masks would be needed.

APPENDIX A

DETAIL OF PROCESS SEQUENCE

A.1 Process Flow

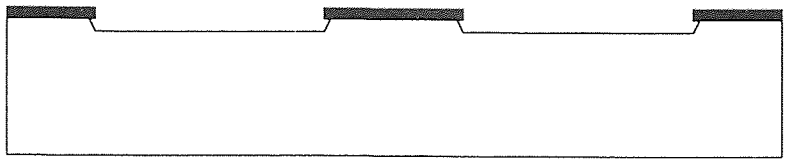

Figure A.1 Patterned silicon nitride isolation and etched well in silicon substrate (process steps 1-15).

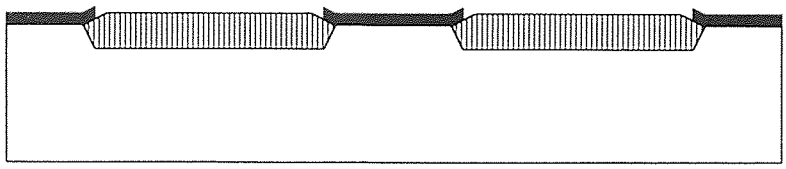

Figure A.2 Completed LOCOS oxidation (process steps 16-25).

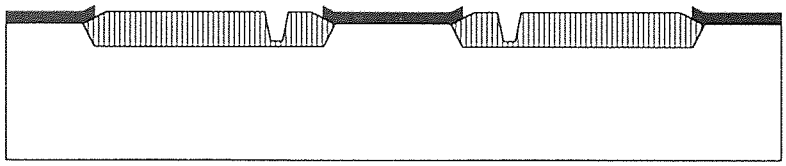

Figure A.3 Mold for rotor support pins etched approximately 90% through LOCOS oxide (process steps 26-38).

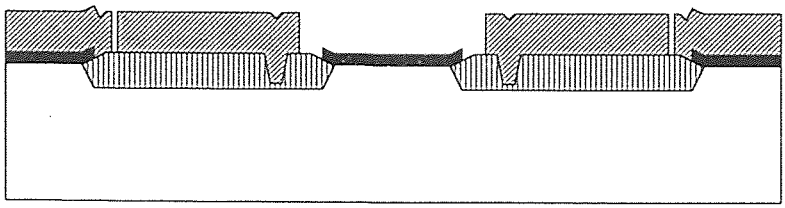

Figure A.4 Deposited and patterned $TaSi_2$ for rotor and stators (process steps 39-52).

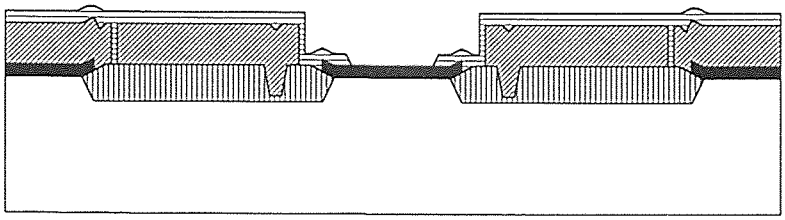

Figure A.5 Deposited and patterned LTO sacrificial layer (process steps 53-68).

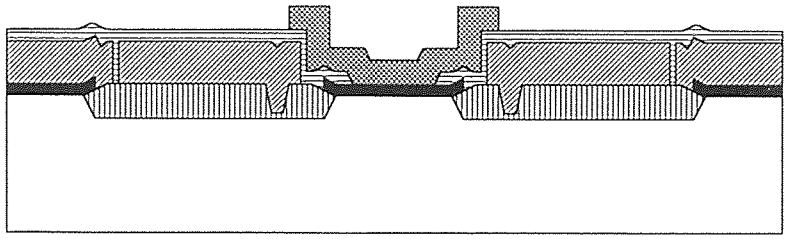

Figure A.6 Deposited and patterned $TaSi_2$ for bearing and stator interconnects (process steps 69-82)

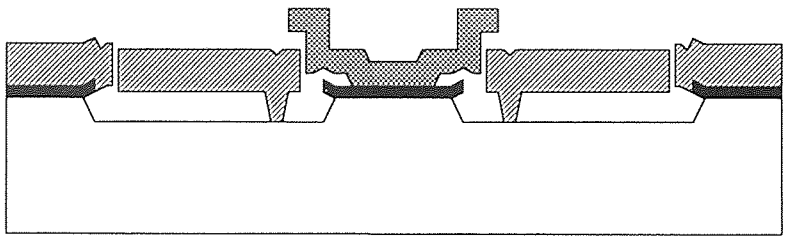

Figure A.7 Completed motor with HF released rotor (process step 83).

A.2 Process Traveler Steps

1. P-clean, 5:1 H_2SO_4 : H_2O_2, 110°C, 10 minutes
2. DI rinse, 5 minutes hot, 5 minutes cold
3. Spin dry
4. Furnace pre-clean, 100:1 HF Dip, 25°C, 1 minute
5. DI rinse, 5 minutes
6. Spin dry
7. Deposit PECVD silicon nitride, 600°C, 5000Å
8. Vapor HMDS, chill, coat wafers with Shipley 3813 photoresist, 4500 RPM, soft bake @ 110°C, 60 seconds
9. Expose photoresist, 10 seconds, mask NITRIDE1
10. Develop 45 seconds with Shipley MF319 developer, hard bake @ 115°C, 60 seconds
11. Plasma etch silicon nitride, 92sccm CF_4, 8sccm O_2, 250mTorr, 25°C, 600Watts, 10 minutes, then measure and adjust remaining etch time accordingly.
12. Plasma etch silicon substrate, 50sccm SF_6, 50sccm C_2ClF_5, 150mTorr, 25°C, 600Watts, 80 seconds.
13. P-strip photoresist, 5:1 H_2SO_4 : H_2O_2, 110°C, 10 minutes
14. DI rinse, 5 minutes hot, 5 minutes cold
15. Spin dry
16. P-clean, 5:1 H_2SO_4 : H_2O_2, 110°C, 10 minutes
17. DI rinse, 5 minutes hot, 5 minutes cold
18. Spin dry
19. Furnace pre-clean, 100:1 HF Dip, 25°C, 1 minute

20. DI rinse, 5 minutes

21. Spin dry

22. Steam oxidation, 2SLM O_2, 750sccm O_2 bubbler, 1000°C, 12 hours

23. Strip oxy-nitride, 100:1 HF Dip, 25°C, 5 minutes

24. DI rinse, 5 minutes

25. Spin dry

26. Vapor HMDS, chill, coat wafers with Shipley 3813 photoresist, 4500 RPM, soft bake @ 110°C, 60 seconds

27. Expose photoresist, 13 seconds, mask OXIDE1

28. Develop 45 seconds with Shipley MF319 developer, hard bake @ 115°C, 60 seconds

29. Etch oxide in 7:1 BOE, 25°C, 8 minutes

30. DI rinse, 5 minutes

31. Spin dry

32. Re-bake photoresist, 115°C, 90 seconds

33. Etch oxide in 7:1 BOE, 25°C, 7 minutes

34. DI rinse, 5 minutes

35. Spin dry

36. P-strip photoresist, 5:1 H_2SO_4 : H_2O_2, 110°C, 10 minutes

37. DI rinse, 5 minutes hot, 5 minutes cold

38. Spin dry

39. P-clean, 5:1 H_2SO_4 : H_2O_2, 110°C, 10 minutes

40. DI rinse, 5 minutes hot, 5 minutes cold

41. Spin dry

42. Furnace pre-clean, 100:1 HF Dip, 25°C, 1 minute

43. DI rinse, 5 minutes

44. Spin dry

45. Deposit $TaSi_2$, 300°C, 3mTorr, 3Å/second, 1.5μm

46. Vapor HMDS, chill, coat wafers with Shipley 3813 photoresist, 4500 RPM, soft bake @ 110°C, 90 seconds

47. Expose photoresist, 12 seconds, mask POLY1

48. Develop 45 seconds with Shipley MF319 developer, hard bake @ 115°C, 60 seconds

49. Plasma etch $TaSi_2$, 75 sccm C_2ClF_5, 25 sccm SF_6, 150 mTorr, 15°C, 600Watts, 45 minutes

50. P-strip photoresist, 5:1 H_2SO_4 : H_2O_2, 110°C, 10 minutes

51. DI rinse, 5 minutes hot, 5 minutes cold

52. Spin dry

53. P-clean, 5:1 H_2SO_4 : H_2O_2, 110°C, 10 minutes

54. DI rinse, 5 minutes hot, 5 minutes cold

55. Spin dry

56. Furnace pre-clean, 100:1 HF Dip, 25°C, 1 minute

57. DI rinse, 5 minutes

58. Spin dry

59. Deposit PECVD LTO, 300°C, 5000Å

60. Vapor HMDS, chill, coat wafers with Shipley 3813 photoresist, 1700 RPM, soft bake @ 110°C, 60 seconds

61. Expose photoresist, 20 seconds, mask OXIDE2

62. Develop 45 seconds with Shipley MF319, hard bake @ 115°C, 60 seconds

63. Etch oxide, 7:1 BOE, 25°C, 2 minutes

64. DI rinse, 5 minutes

65. Spin dry

66. P-strip photoresist, 5:1 H_2SO_4 : H_2O_2, 110°C, 10 minutes

67. DI rinse, 5 minutes hot, 5 minutes cold

68. Spin dry

69. P-clean, 5:1 H_2SO_4 : H_2O_2, 110°C, 10 minutes

70. DI rinse, 5 minutes hot, 5 minutes cold

71. Spin dry

72. Furnace pre-clean, 100:1 HF Dip, 25°C, 1 minute

73. DI rinse, 5 minutes

74. Spin dry

75. Deposit $TaSi_2$, 300°C, 3mTorr, 3Å/second, 1.0μm

76. Vapor HMDS, chill, coat wafers with Shipley 3813 photoresist, 1000 RPM, soft bake @ 110°C, 60 seconds

77. Expose photoresist, 33 seconds, mask POLY2

78. Develop 45 seconds with Shipley MF319, hard bake @ 110°C, 90 seconds

79. Plasma etch $TaSi_2$, 75sccm C_2ClF_5, 25sccm SF_6, 150mTorr, 15°C, 600Watts, 35 minutes

80. P-strip photoresist, 5:1 H_2SO_4 : H_2O_2, 110°C, 10 minutes

81. DI rinse, 5 minutes hot, 5 minutes cold

82. Spin dry

83. Sacrificial oxide release etch

APPENDIX B

PHYSICAL DESIGN - GRAPHICAL LAYOUT

The mask layouts for each level of the micromotors are shown in figures B.1 through B.5. The stacked mask layout for an entire micromotor is shown in figure B.6.

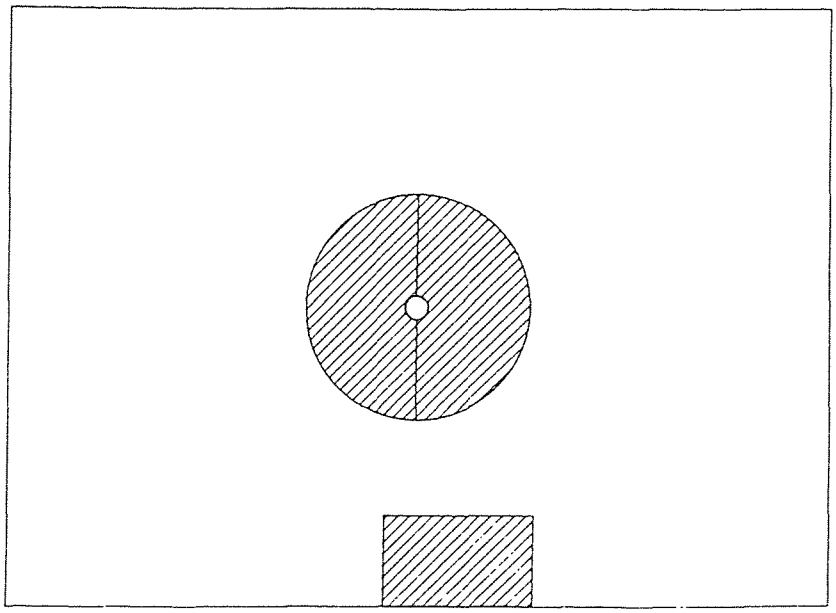

Figure B.1 NITRIDE1 mask geometry (clear feature/opaque background)

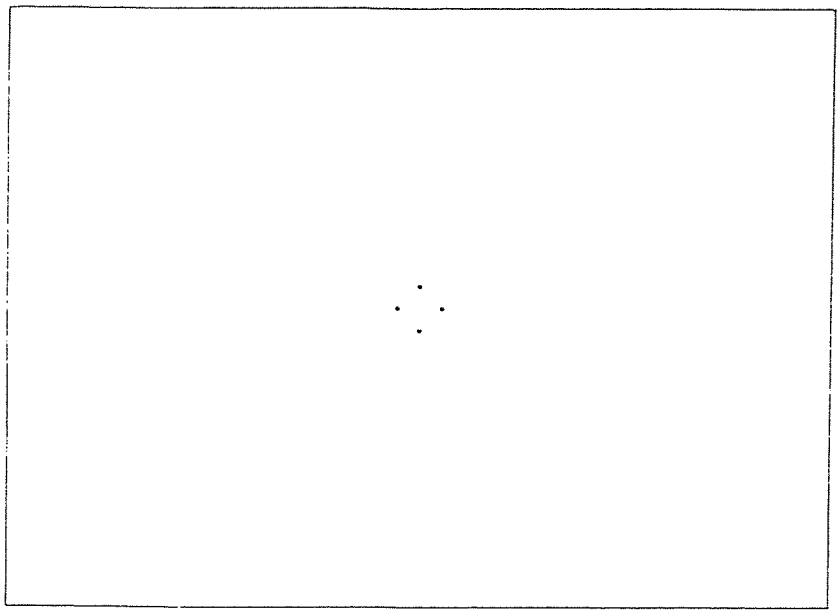

Figure B.2 OXIDE1 mask geometry (clear feature/opaque background)

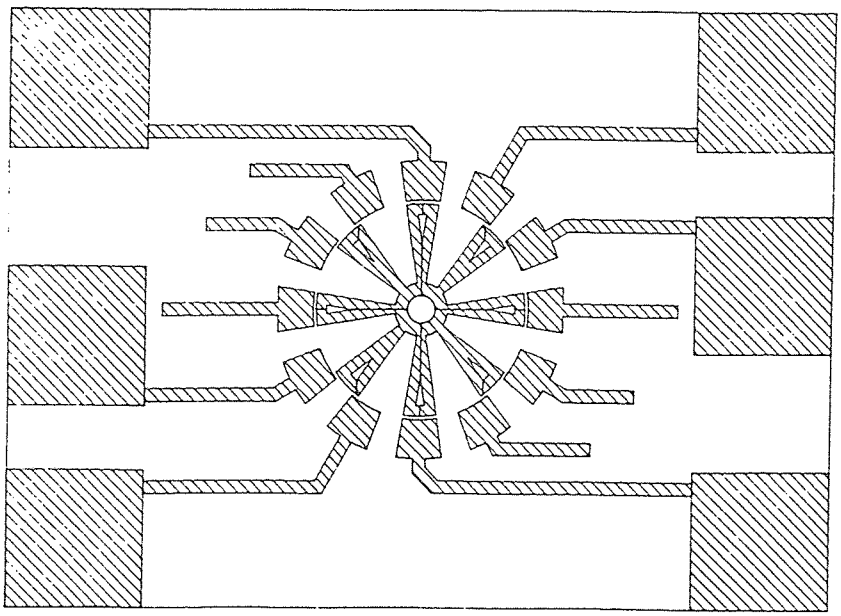

Figure B.3 POLY1 mask geometry (opaque feature/clear background)

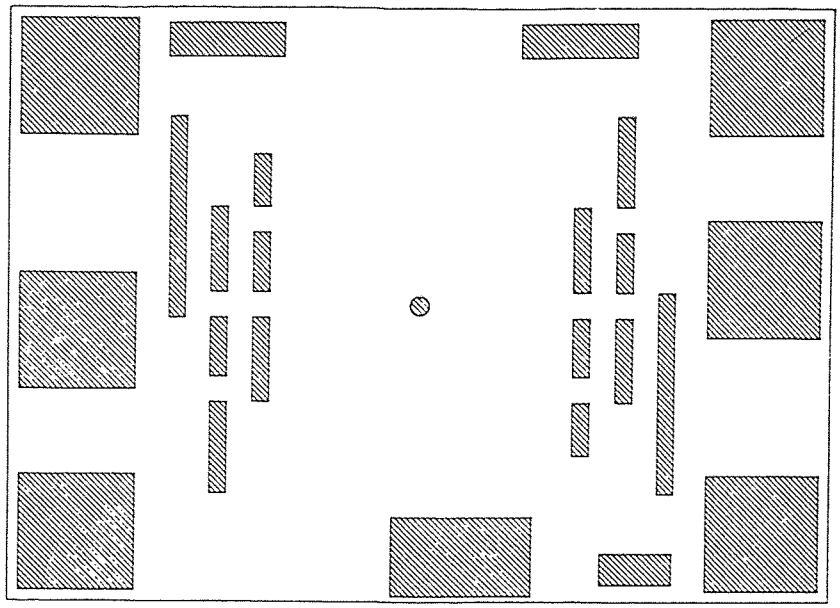

Figure B.4 OXIDE2 mask geometry (clear feature/opaque background)

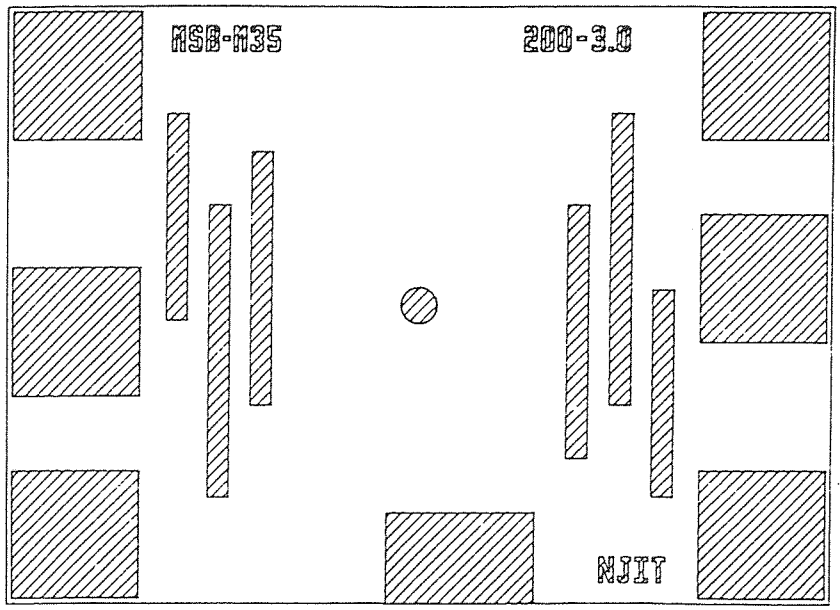

Figure B.5 POLY2 mask geometry (opaque feature/clear background)

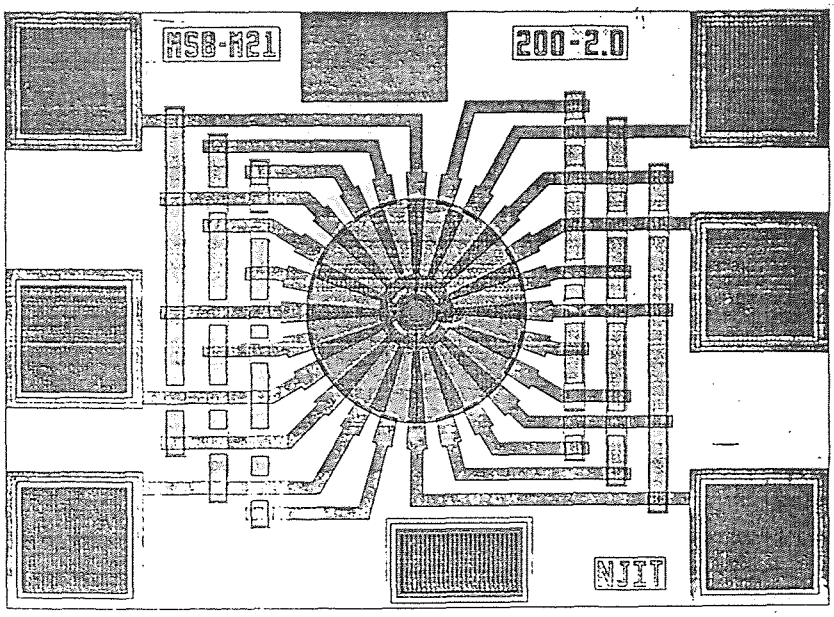

Figure B.6 Complete stacked mask set.

APPENDIX C

MOTOR PARAMETERS

The specific motor geometry that provides the best motor performance is not easily determined by simulation alone. Accurate simulation of the motors requires a 3 dimensional simulator, due to the fringing electric fields present in all planes of the motors. One way of determining the better design geometries is to actually fabricate several variations of the motors and determine their relative performance by experimental tests.

This work uses simulations of previous works as a basis for the designs of the motors, and includes several permutations of the pertinent design parameters. Tabulated below are 18 unique geometries with variables including rotor diameter R, number of stator poles and rotor poles P_S:P_R, rotor pole width θ_R, stator pole width θ_S, bearing diameter R_B, and bushing type (4 dots or ring). For each of the 18 designs, there are motors on the mask set with 1, 2, and 3μm rotor-stator gaps, for a total of 54 motors.

Table C.1 Pertinent design parameters for the micromotors. Each set of parameters applies to motors with 1, 2, and 3μm rotor/stator gaps, for a total of 54 unique geometries.

R (μm)	P_S:P_R	θ_R (°)	θ_S (°)	R_B (μm)	Bushing*
100	6:4	36	36	26	dots
150	6:4	36	36	26	dots
200	6:4	36	36	26	dots
100	12:8	18	18	26	dots
150	12:8	18	18	26	dots
200	12:8	18	18	26	dots
100	12:8	18	18	16	dots
150	12:8	18	18	16	dots
100	12:8	18	18	26	ring
150	12:8	18	18	26	ring
100	12:8	18	27	26	dots
100	24:8	27	12	26	dots
150	24:8	27	12	26	dots
200	24:8	27	12	26	dots
100	24:8	12	12	26	dots
100	24:16	9	9	26	dots
150	24:16	9	9	26	dots
200	24:16	9	9	26	dots

*Dots refers to four 3μm (nominal) diameter support pins; ring refers to a 3μm wide ring, concentric with the center bushing, for vertical rotor support.

REFERENCES

1 Y.C. Tai, L.S. Fan, and R.S. Muller. *IC*-Processed micro-motors: design, technology, and testing. *Proceedings of IEEE Micro Electro Mechanical Systems: An Investigation of Micro Structures, Sensors, Actuators, Machines and Robots*, pages 1-6, Salt Lake City, UT, February 20-22, 1989.

2 M. Mehregany, S.F. Bart, L.S. Tavrow, J.H. Lang, S.D. Senturia, and M.F. Schlecht. A study of three microfabricated variable-capacitance motors. *Transducers '89: Proceedings of the 5th International Conference on Solid-State Sensors and Actuators and Eurosensors III*, pages 173-179, Montreux, Switzerland, June 25-30, 1989.

3 M. Mehregany, P. Nagarkar, S.D. Senturia, and J.H. Lang. Operation of microfabricated harmonic and ordinary side-drive motors. *Proceedings of IEEE Micro Electro Mechanical Systems: An Investigation of Micro Structures, Sensors, Actuators, Machines and Robots,* pages 1-8, Napa Valley, CA, February 11-14, 1990.

4 M. Mehregany, S.F. Bart, L.S. Tavrow, J.H. Lang, and S.D. Senturia. Principles in design and microfabrication of variable-capacitance side-drive motors. *Journal of Vacuum Science and Technology*, A 8(4):3614-3624, Jul.-Aug. 1990.

5 L.S. Tavrow. *A LOCOS-Based Microfabricated Radial-Gap Electric Motor.* Ph.D. thesis, Massachusetts Institute of Technology, 1991.

6 M. Mehregany. *Microfabricated Silicon Electric Mechanisms.* Ph.D. thesis, Massachusetts Institute of Technology, 1990.

7 G. Stix. Micron Machinations. *Scientific American*, November 1992, pp. 106-117.

8 Y.C. Tai. *IC-Processed Polysilicon Micromechanics: Technology, Material, and Devices.* Ph.D. thesis, University of California at Berkeley, 1989.

9 L.S. Fan. *Integrated Micromachinery -- Moving Structures on Silicon Chips.* Ph.D. thesis, University of California and Berkeley, 1990.

10 S.F. Bart. *Modeling and Design of Electroquasistatic Microactuators.* Ph.D. thesis, Massachusetts Institute of Technology, 1990.

11 H. Yu. *Rotary Micromotor Design with IC-Compatible Processing.* Master's thesis, New Jersey Institute of Technology, 1990.

12 Y.C. Tai and R.S. Muller. Frictional Study of IC-processed Micromotors. *Transducers '89: Proceedings of the 5th International Conference on Solid-State Sensors and Actuators and Eurosensors III*, pages 180-183, Montreux, Switzerland, June 25-30, 1989.

13 S.M. Sze. *Semiconductor Devices: Physics and Technology*. John Wiley and Sons, New York, 1985.

14 Anonymous. *DRIE-100/102 Operation Manual.* General Signal/Drytek, Wilmington, MA, 1983.

15 Anonymous. *Plasma II / AMP 3300 Plasma Deposition System Manual.* Applied Materials, Santa Clara, CA, 1979.

16 S. Wolf and R.N. Tauber. *Silicon Processing for the VLSI Era: Volume 1 - Process Technology*. Lattice Press, Sunset Beach, CA, 1986.

17 J.T. Pan and Ilan Blech. In situ stress measurement of refractory metal silicides during sintering. *Journal of Applied Physics*, **55**(8):2874 - 2880, 15 April 1984.

18 J. Angilello, J.E.E. Baglin, F. Cardone, J.J. Dempsey, F.M. d'Heurle, E.A. Irene, R. MacInnes, C.S. Petersson, R. Savoy, A.P. Segmuller, and E. Tierney. Tantalum Silicide Deposited by Sputtering. *Journal of Electronic Materials*, 10:59 - 71, 1981.

19 Durga Misra, Jong Kim, and William N. Carr. Anisotropic reactive ion etching of tantalum silicide films in CF_4 + O_2 plasma for micromechanical structures. *Proceedings of the Second International Conference on Electronic Materials*, pages 415 - 420, Newark, New Jersey, USA, Sept. 17-19, 1990.

20 W. Beinvogl and B. Hasler. Reactive Ion Etching of Polysilicon and Tantalum Silicide. *Solid State Technology*, pages 125-130, April 1983.

21 Stephen E. Clark, J.-K. Tsang, and James W. Marolf. Deposition and Patterning of Tungsten and Tantalum Polycides. *Solid State Technology*, pages 235-242, April 1984.

22 Johanson Manufacturing Corporation. Product brochure 6CAJ5M9C1 for RF/Microwave Trimmer Capacitors and Tuning Devices.

23 S. P. Murarka. *Silicides for VLSI Applications*. Academic Press, New York, NY, 1983.

24 M. S. Phadke, R. N. Kackar, D. V. Speeney, and M. J. Grieco. Off-Line Quality Control in Integrated Circuit Fabrication Using Experimental Design. *The Bell System Technical Journal*, pages 1273-1309, May-June 1983.